Materials Research Laboratory, Inc.

One Science Road
Glenwood, Illinois 60425

♦ Area Code 312
♦ Local telephone 755-8780
♦ Chicago telephone 785-4020

FINAL REPORT

on

FRACTURE OF METAL-ADHESIVE-COMPOSITE AND COMPOSITE-ADHESIVE-COMPOSITE SYSTEMS

Contract No. NAS3-21824
MRL No. 534

For

NATIONAL AERONAUTICS AND SPACE ADMINISTRATION
Lewis Research Center
Cleveland, OH 44135

By

E. J. Ripling and J. S. Santner

October 1980

Materials
Research
Laboratory,
Inc.

FINAL REPORT

on

FRACTURE OF METAL-ADHESIVE-COMPOSITE AND COMPOSITE-ADHESIVE-COMPOSITE SYSTEMS

Contract No. NAS3-21824
MRL No. 534

For

NATIONAL AERONAUTICS AND SPACE ADMINISTRATION
Lewis Research Center
Cleveland, OH 44135

By

E. J. Ripling and J. S. Santner

October 1980

ABSTRACT

This program was undertaken to initiate the development of a test method for testing adhesive joints in metal-adhesive-composite and composite-adhesive-composite systems. The uniform double cantilever beam (UDCB) and the width tapered beam (WTB) specimen geometries were evaluated for measuring Mode I fracture toughness in these systems. The WTB specimen is the preferred geometry in spite of the fact that it is more costly to machine than the UDCB specimen.

The use of loading tabs attached to thin sheets of composites proved to be experimentally unsatisfactory. Consequently, a new system was developed to load thin sheets of adherends. This system allows for the direct measurement of displacement along the load line.

In well made joints separation occurred between the plies rather than in the adhesive.

FOREWORD

The study reported in this program was conducted by the Materials Research Laboratory, Inc., of Glenwood, Illinois, and was sponsored by the National Aeronautics and Space Administration through the Lewis Research Center under Contract No. NAS3-21824.

W. F. Brown, Jr., was the NASA Technical Monitor, with E. J. Ripling as the MRL Program Manager and Principal Investigator. J. S. Santner was Technical Investigator. The specimen bonding and mechanical testing was conducted by K. O'Donnell. P. B. Crosley is responsible for the analytical development of Appendices A and B.

NOMENCLATURE

A	beam cross section area
a	crack length for a double cantilever beam (DCB) fracture specimen measured from the point of loading to the end of the cracked region.
a_i	initial starter flaw length in a DCB specimen
a_o	coefficient used to describe the change of apparent tensile modulus as a crack grows in a DCB specimen
b	crack front length
B	maximum specimen width for a width tapered beam specimen
C	specimen compliance (displacement per unit load)
C'	rate of change of specimen compliance with crack length, dC/da
D	depth of a 3-point bend specimen (same as h in a DCB fracture specimen)
DCB	double cantilever beam
E	tensile modulus
E_o	coefficient used to describe the change of apparent tensile modulus as the span-to-depth increases for a three-point bend specimen
$\mathcal{G}$	crack extension force
h	height of one beam for a double cantilever beam fracture specimen
I	moment of inertia
k	ratio of a/b for a width tapered beam (WTB) specimen
M	bending moment (Px)
P	load applied to a specimen
S	distance between support for a three-point bend specimen

NOMENCLATURE, Continued

V	opening measured at the load line for a double cantilever beam fracture specimen
W	length of a double cantilever beam fracture specimen from the center of loading to the end of the specimen in the direction of the crack growth
u	span-to-depth ratio (S/D) for a three-point bend specimen
x	spatial coordinate in appendix
UDCB	uniform double cantilever beam fracture specimen
WTB	width tapered beam fracture specimen
y	spatial coordinate in appendix
α, β	coefficients for a linear least squares regression relating compliance and crack length
θ	coefficient relating load to crack extension force for a width tapered beam fracture specimen
$\mathscr{H}$	constant of integration
ρ	coefficient relating crack length to load for a uniform double cantilever beam fracture specimen
ν	Poisson's ratio
ϕ	correction factor to the DCB specimen behavior when the crack length dependent tensile modulus is considered

TABLE OF CONTENTS

TABLE OF CONTENTS, Continued

LIST OF TABLES

LIST OF ILLUSTRATIONS

LIST OF ILLUSTRATIONS, Continued

Materials
Research
Laboratory,
Inc.

FRACTURE OF METAL-ADHESIVE-COMPOSITE AND COMPOSITE-ADHESIVE-COMPOSITES

1. Introduction

Adhesive joints fracture by the propagation of crack-like defects, such as unbonded areas, that occur in the glue-line. Fractures of this kind have been studied for more than a dozen years at the Materials Research Laboratory, primarily by Mostovoy and Ripling. These studies described the behavior of metal-adhesive-metal (MAM) systems under a number of loading conditions including continuously increasing loads, alernating load and sustained loads[1]. The behavior of a large number of adhesives was catalogued as a function of joint geometry, test temperature, and environment[2], and it was demonstrated that laboratory test data could be used to predict the fracturing characteristics of complex structures[3]. An ASTM Test Method for measuring the fracture mechanics parameters of adhesive bonds was developed[4] on the basis of these studies.

Progressive separations of the type found in MAM systems are also expected in systems in which one of both of the adherends is a composite. Hence, the study of joint fractures has been extended to include composite adherends. One major reason for carrying out this study was to determine whether or not the test methods developed for metal adherend systems could be extended to include composites, either as composite-adhesive-composite (CAC) or as metal-adhesive-composite (MAC) hybrid systems.

Metal and composite adherends are expected to act differently, and, in general, metal adherend systems are probably easier to classify than composite adherend systems. In most adhesive tests, cracking is produced by elastically bending the adherends so that the elastic modulus of the adherend must be known to measure the toughness of the adhesive. The elastic modulus is essentially constant for a single type of homogeneous metals, such as aluminum alloys. For composites it is not only a function of the reinforcement and matrix species, but also of the lay-up pattern. Second,

the apparent bending modulus of metals is only dependent on the beam span-to-height ratio when it is small, while in composites the apparent bending modulus is constant only when the ratio is very large. Finally, and most important, the through-the-thickness toughness of composites is much lower than it is for metals. Hence, for metal adherends, the crack that is initiated in the adhesive is not able to wander into the adherends; this is not the case for composite adherends[8]. These differences place restrictions on specimens designed to measure the fracture mechanics parameters in composite-adherend systems.

2. Test Materials and Specimen Analysis

2.1 Test Materials

Two composites were used in this study: both were graphite/epoxy sheets, nominally 0.125 inch (3mm) thick, having the same number of cross-plies. The ply lay-up, the number of fiber orientations, and total number of plies are given in Table I. Composite A was fabricated to have the 0° plies near the sheet center, where bending stresses are at a minimum, while for composite B the 0° plies were near the surface, where bending stresses are greatest. The two different lay-up patterns were selected so that the two composites would have different flexure moduli.

The adhesive AF-163-2k (0.06 oz/ft^2) utilized in this program is manufactured by the Minnesota Mining and Manufacturing Company. It is a 250F (120C) curing adhesive reported to have excellent water resistance. This lower temperature curing adhesive was selected rather than the 350F (175C) curing ones normally used with composites so that the aluminum adherends could be used without significantly altering their yield strength. The adhesive is generically a modified epoxy.

2.2 Specimen Type and Analysis

As was the case for the MAM specimens in Method D3433-75[4], double cantilever beam specimens were selected for this program. Both the uniform height double cantilever beam (UDCB) specimen and the width tapered beam (WTB) specimen were used. Preliminary experiments were conducted

Table I

DESIGN OF COMPOSITE ADHERENDS

Designation	Total No. of Plies	No of Cross Plies	Lay-up Sequence
A	21	4	$[+45/-45/0/90/0/-45/+45]_3$
B	21	4	$[0_3/+45_3/-45_3/90_3/-45_3/+45_3/0_3]$

on the UDCB specimen. Its geometry is simpler than the WTB specimen geometry and allows the efficient utilization of composite material. The WTB specimen, unlike the UDCB, has the advantage that $\mathcal{G}$ is independent of crack length, and hence its measurement only requires that load be monitored. Unfortunately, it is somewhat more expensive than a UDCB specimen, but its advantage in stress corrosion cracking and fatigue are so great that this additional expense is justified. Both specimen types can be produced by "wide-area" bonding.

2.3 Analysis of DCB Specimens

Both the UDCB and WTB specimens have been analyzed earlier[5-8]. However, in using composite adherends it is advantageous to select the adherend thickness so that neither the rotation correction given in ref. (6) nor the large displacement expression given in (7) are needed. Hence, the simplified expression for the crack extension force, $\mathcal{G}$, as given below, is adequate.

For any specimen or structure the compliance, C, and load, P, are related to $\mathcal{G}$ by the expression

$$\mathcal{G} = P^2C'/(2b) \qquad (2\text{-}1)$$

where $C' = dC/da$, the rate of change of compliance with crack length, and b is the specimen thickness at the crack front position. The compliance at the loading point is the displacement per unit load, i.e., $C = V/P$ where V is the load point displacement. The present concern is the relation between P and V for a crack extending at constant $\mathcal{G}$. The desired relation is obtained by substituting the quantity $P = V/C$ for P in eq. (2-1). This gives

$$P = (2bC\mathcal{G}/C')\cdot(1/V) \qquad (2\text{-}2)$$

For a DCB specimen analyzed as a pair of built-in beams which deform by bending, the compliance change is given by

$$C' = \frac{2a^2}{EI} \qquad (2\text{-}3)$$

where a is the crack length measured from the load line, E is Young's

modulus, and I is the moment of inertia of the beam cross section at the crack front position.* For rectangular cross sections

$$C' = 24\, a^2/(Ebh^3) \qquad (2\text{-}4)$$

The compliance can be obtained by carrying out the integration

$$C = C_o + \int_o^a C'\, da \qquad (2\text{-}5)$$

where C_o can be formally identified as the compliance corresponding to $a = 0$. The integration will depend on the variation with crack length of the beam cross section and of Young's modulus**. The simplest case is the uniform DCB specimen where b and h are independent of a, and the integration gives

$$C = 8a^3/(Ebh^3) \qquad (2\text{-}6)$$

assuming that C_o makes a negligible contribution to the compliance. Substituting eqs. (2-4) and (2-6) into eq. (2-2) gives the load-displacement relationship for the uniform DCB specimen:

$$P = (2ab\ell/3)\cdot(1/V) \qquad (2\text{-}7)$$

A second type of specimen used on this program was the width-tapered-beam (WTB) specimen in which the thickness, b, increases linearly with the crack length, a; i.e., $b = a/k$ where k is constant. Carrying out the integration indicated in eq. (2-5) gives

$$C = C_o + [12k/(Eh^3)]\cdot a^2 \qquad (2\text{-}8)$$

Since beam theory is not exact, measured compliance values may differ from eq. (2-8). The procedure then is to fit the experimental compliance data to an equation of the form

$$C = \beta + \alpha a^2 \qquad (2\text{-}9)$$

---

* This result is derived in Appendix A.

** In the composite materials tested on this program the apparent elastic modulus in bending depends on beam length. This situation is addressed in Appendix B.

In eq. (2-9) β can be identified with C_o and α is simply a parameter fitted to experimental compliance data. If the beam model were precisely applicable, α would have a value corresponding to $12k/(Eh^3)$; in fact, it might be somewhat different. The compliance derivative, C', obtained from eq. (2-9) is

$$C' = 2\alpha a = 2\alpha kb \qquad (2\text{-}10)$$

and substitution of this value into eq. (2-1) gives

$$\mathcal{G} = P^2 \alpha k \qquad (2\text{-}11)$$

To the extent that a single value of α provides a good fit to the compliance data over a range of crack lengths, the relation between $\mathcal{G}$ and P is independent of crack length in that range.

3. Test Results

3.1 Three-Point Bend Measurement of Tensile Modulus for Composites A and B

One difficulty encountered in testing DCB specimens with composite adherends, is that the apparent elastic modulus of composites loaded in bending can depend on the adherends span-to-depth ratio. The results of a recent survey[9] suggest that a span-to-depth ratio of at least 30/1 may be necessary to avoid this effect. As the design and analysis of DCB specimens must take this modulus variation into account, measurements were made on the materials used in this program. Three-point bend specimen tests were conducted according to the ASTM Standard D790[10]. Two series of tests were run to determine whether the modulus was affected by specimen width, b. In the first series, specimens were 0.5 inch (12.7 mm) wide, and in the second, the specimen width was increased to 1.0 inch (25.4 mm). Figure 1 is a plot of the apparent tensile modulus measured as a function of the span-to-depth (S/D) ratio for the specimens with two different widths. The modulus is seen to be independent of width for both composites tested. As expected, placing the 0° plies near the surface of composite B significantly increased its stiffness over composite A, where the

0° plies were located more uniformly throughout the thickness. In addition, the apparent modulus reached a plateau with 90 percent of the saturated value, E_o, near the S/D ratio of 30/1. Composite A reached its 90 percent of the plateau value at a smaller S/D ratio (20/1).

In order to model these effects in the UDCB and WTB specimen geometries, the apparent modulus must be expressed as a function of the crack length, i.e., E = E(a). Several empirical fitting functions having the general shape of Fig. 1 were investigated. The best fit was obtained with:

$$E = E_o (1 - u_o/u), \; u = S/D \tag{3-1}$$

which has a correlation coefficient of better than 0.98 for both composites. In order to relate the crack length, a, in a double cantilever beam to the span in a three-point bend test, the following identifications are made:

$$\frac{S}{2} \rightarrow a, \; \frac{S_o}{2} \rightarrow a_o, \; u = \frac{S}{D}, \text{ and } u_o = \frac{S_o}{D} \tag{3-2}$$

so that,

$$a_o = \frac{u_o D}{2}, \text{ and } \frac{u_o}{u} \rightarrow \frac{a_o}{a} \tag{3-3}$$

Based on the observations for two extremes of composite structure and the correlations between a three-point bend specimen and a double cantilever beam specimen, the requirements for initial crack length were established. A span-to-depth ratio of 30/1 for a three-point beam is equivalent to a ratio of 15/1 for a cantilever beam. Since the composites used in the program were .125 inch (3 mm) thick, the initial crack length, a, should be almost two inches (50 mm) long. The initial blunt starter flaw was made shorter than this to allow room for it to jump to form a natural crack on loading. While data is collected for a/h < 15, it is not considered valid until it extends beyond this region. In designing the test specimens for this program, the starter cracks were made to equal about one-half the required value of a/h. In this way, both the specimen size and magnitude of displacements that had to be measured were reduced to manageable sizes. The critical value of a/h = 15 is marked on the test records (Figs. 3, 4, 12 and 13).

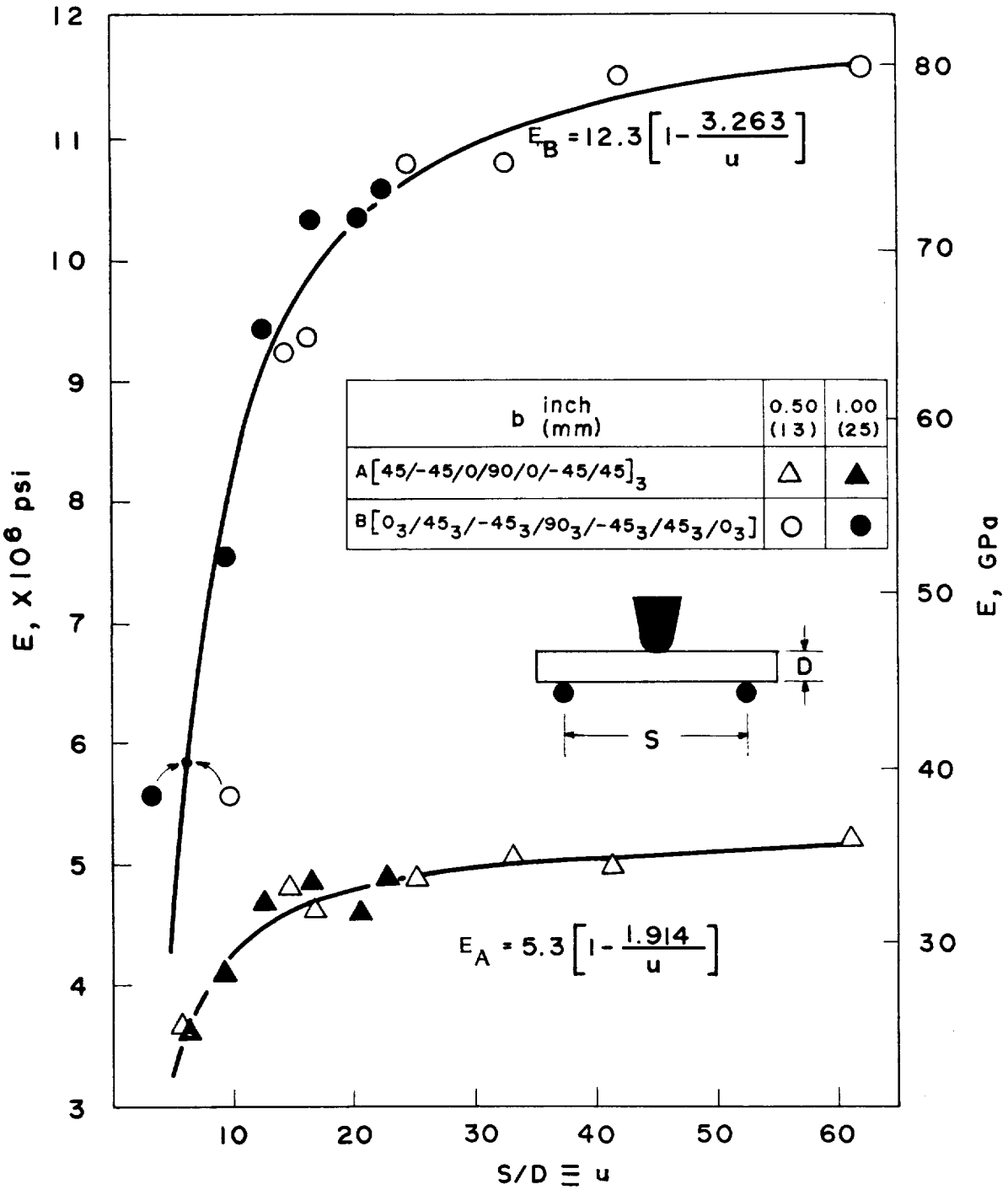

Fig. 1 Apparent modulus as a function of span-to-depth ratio, u.

3.2 UDCB Specimen

3.2.1 Specimen Shape

Uniform double cantilever beam specimens with the geometry in Fig. 2 were fabricated for testing. Individual oversized specimen blanks, approximately 7/8 x 4 inch (22 x 100 mm), were bonded together following the manufacturer's recommended procedure, with the exception of pressure. This value was decreased by half to minimize excessive adhesive run-out experienced during gluing trials with unidirectionally reinforced composites. The purpose of these trials was to establish the characteristic failure mode with composite adherends, and determine the feasibility of measuring adhesive toughness with the UDCB specimen.

3.2.2 Test Results of UDCB Specimen

Typical load-deflection test records from UDCB specimens with composite A and composite B adherends are shown in Figs. 3 and 4, respectively. Both figures show non-linearity associated with the initial loading. In addition, whenever the tests were interrupted to optically measure the crack length, the load decreased by 7-10 percent. This might be due to plastic flow at the crack tip, or slow, subcritical crack extension. No arrest marks or similar features were observed at those locations using optical fractography up to 50X magnification. Upon continuing the test, the load monotonically increased until the pre-interrupted loads were reached. Further work is needed to understand how sensitive $\mathcal{G}$ is to loading rates.

The broken line in Fig. 3 is the P-V curve for $\mathcal{G}$ = 1.0 lb/in (174 N/m) calculated from eq. (2-7). The theoretical curve beyond the initial non-linearity closely matches the experimental line, if the interrupted portion of the test is neglected. The low value of $\mathcal{G}$ is due to the fact that this specimen failed by adhesive failure, i.e., separation at the adhesive-composite interface.

Following the same procedure for the curve in Fig. 4, which is a specimen with B composite adherend, such good agreement was not found. This is due to the fact that the fracture mode changed after the test was

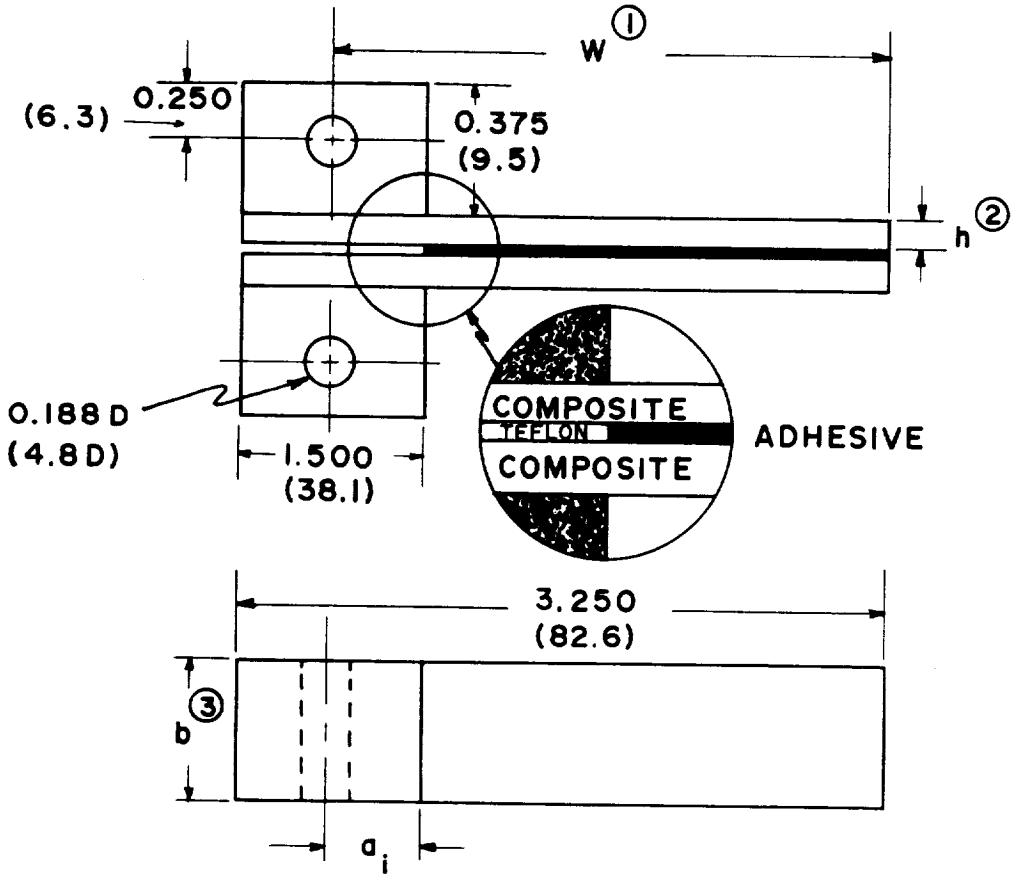

NOTES: ① W = 3.000 (76.2)
② h = 0.125 (3.2)
③ b = 0.750 (19.0)

Fig. 2 UDCB specimen geometry with W/h = 24. All dimensions are inches (mm).

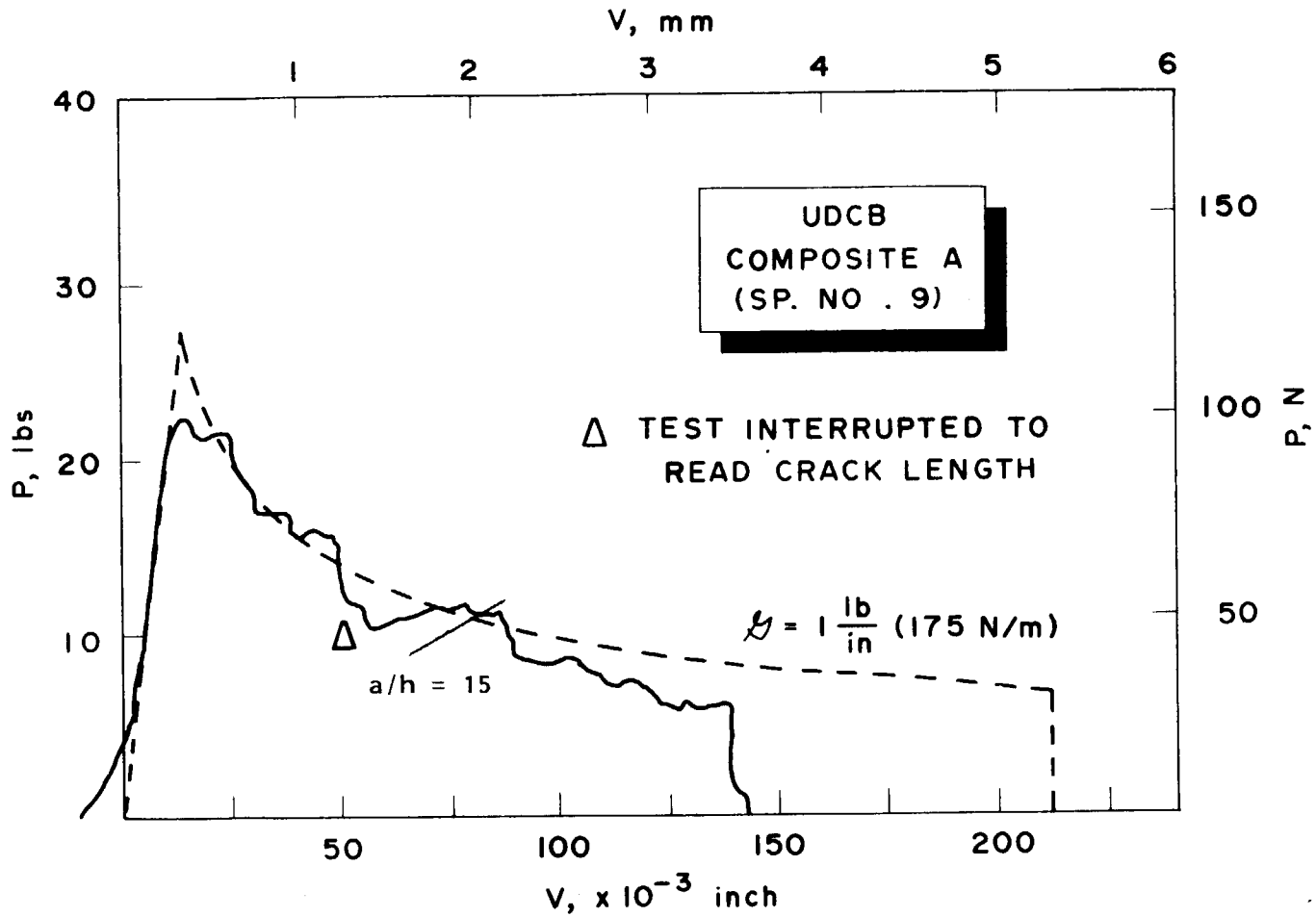

Fig. 3 Typical load-deflection curve for similar composite adherends whose failure mode is 100% adhesive failure, i.e., separation at the adhesive-composite interface.

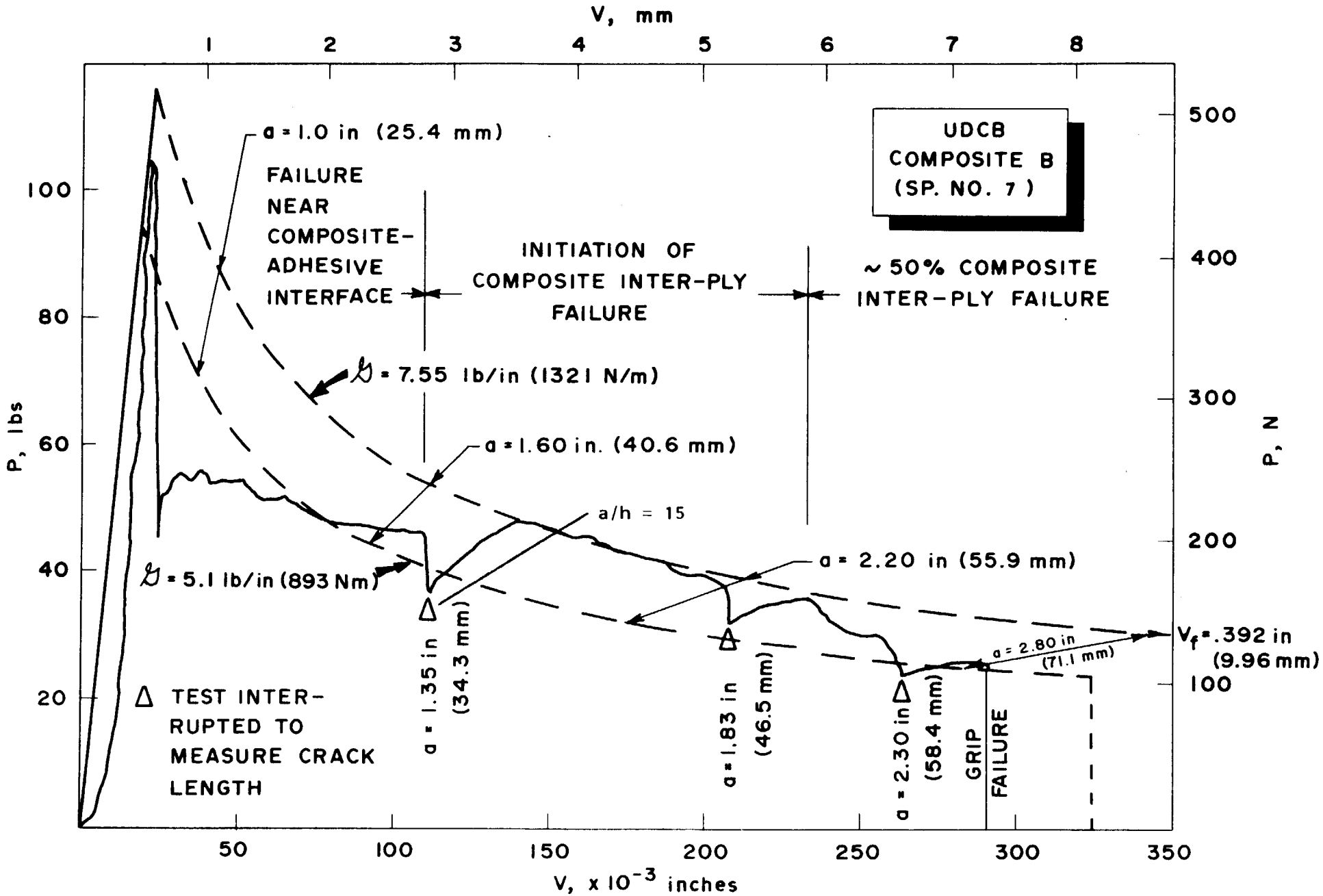

Fig. 4 Experimental load-deflection curve for similar composite adherends whose failure mode gradually changes.

stopped to measure the crack length. Failure near the adhesive-composite interface was the primary failure mode until the crack grew to 1.35 inches (34.3 mm). At this point the test was interrupted to measure the crack length. After this interruption, the failure mode changed to include inter-ply separation along one edge of the crack front. The test was interrupted again at a crack length of 1.83 inches (46.5 mm). Approximately half of the crack front failed by inter-ply separation, and the remainder of the crack front continued to fail near the composite-adhesive interface when the crack length reached two inches. Since interrupting the test to measure the crack length is associated with a change in the fracture mode, this procedure appeared to be a questionable practice. Figure 5 shows the macro fracture surfaces of the specimens, which are summarized in Table II.

3.3 WTB Specimen

Evaluating the fracture toughness using the UDCB specimen requires the simultaneous measurement of the load and crack length. As noted in the previous section, interrupting a UDCB specimen test to measure the crack length may cause transients to occur. This raises questions of interpreting the test record. The geometry of the WTB specimen is designed so that only knowledge of the load is required to measure $\mathcal{G}$.

3.3.1 Loading Thin Adherend Panels

Loading thin (0.125 inch, i.e., 3.2 mm) adherends with externally attached tabs such as shown in Fig. 2, was not a satisfactory experimental arrangement. Separately attaching tabs is an expensive, time consuming process, in which frequent tab failure was experienced. In addition, while several procedures for assuring pin hole alignment were tried, none were completely satisfactory. Therefore, a new approach for loading thin adherend specimens, illustrated in Fig. 6, was devised which could be applied to either a UDCB specimen or a WTB specimen. However, in the present program, this approach was used only on WTB specimens with the geometry illustrated in Fig. 7.

The unique feature of this loading arrangement was the use of the same member for applying the load and measuring displacement. In this

Fig. 5a Fractographs of UDCB specimens with matching A composite adherends.

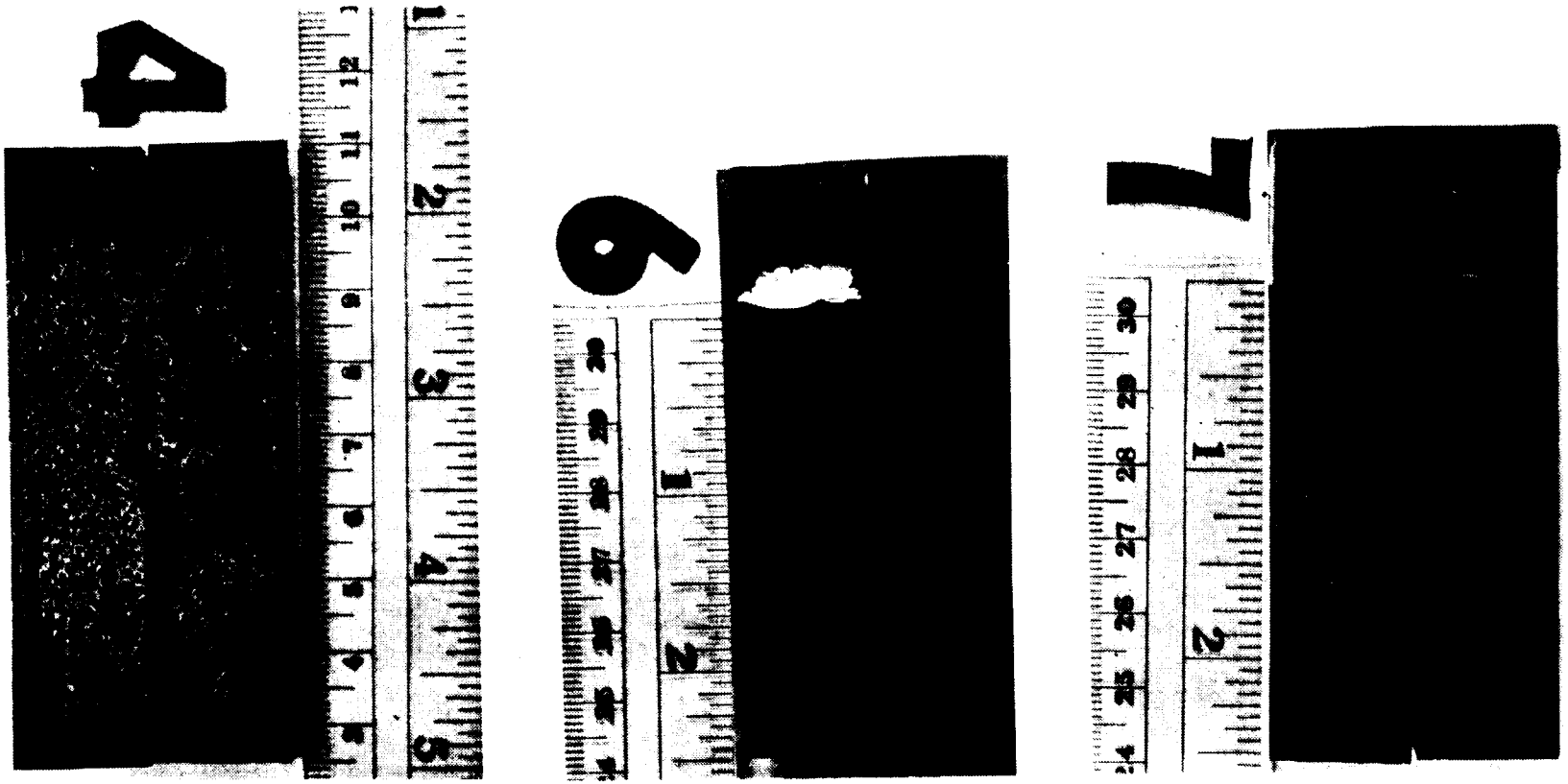

Fig. 5b Fractographs of UDCB specimens with matching B composite adherends.

Table II

UDCB SPECIMEN TEST RESULTS

Spec. No.	Adherend	Bond Line Thickness mils (mm)	Failure Mode*
4	B	9 (0.23)	CF (a/h < 24)/BF (0°) [on edges for (a/h < 24)]
6	B	6 (0.15)	AF (a/h < 24)
7	B	4 (0.10)	CF (a/h < 16)/BF (0°) [a/h > 16]
5	A	5 (0.13)	AF (a/h < 16)/BF (0°) [a/h > 16]
8	A	5 (0.13)	AF (a/h < 24)/BF (0°) [7.2 < a/h < 9.1]
9	A	6 (0.15)	AF (a/h < 24)

*Failure modes in adhesive tests.

Failure Mode	Description
AF	Adhesive failure: separation at the adhesive-adherend interface.
BF (x°)	Beam failure: failure of the adherend.
	(x = 90°: fracture of the beam arm perpendicular to the bond line.
	(x = 0°: fracture of the beam arm parallel to the bond line (inter-ply separation for composite adherends).
CF	Cohesive failure in the center of the bond line.

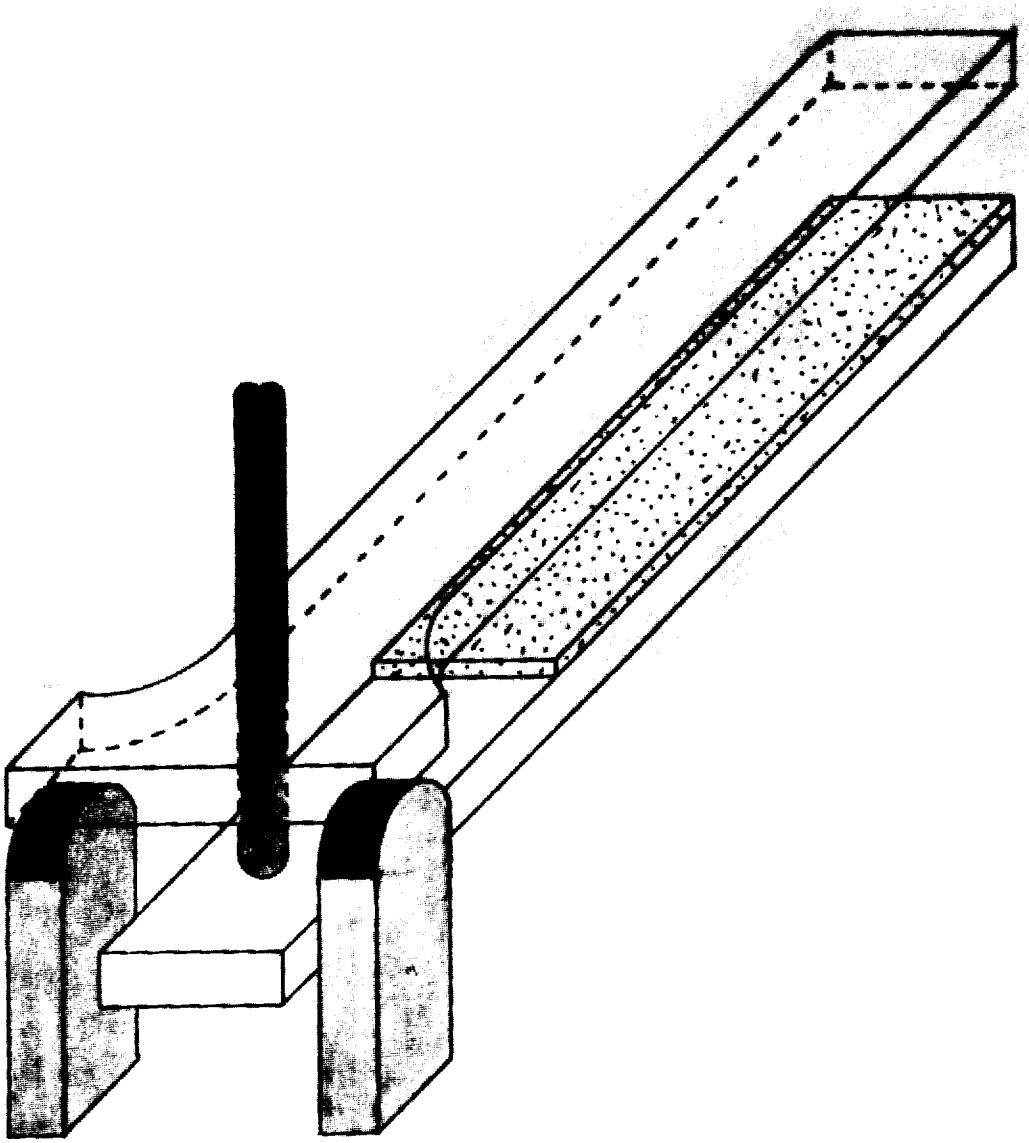

Fig. 6 Loading concept for thin adherend specimens.

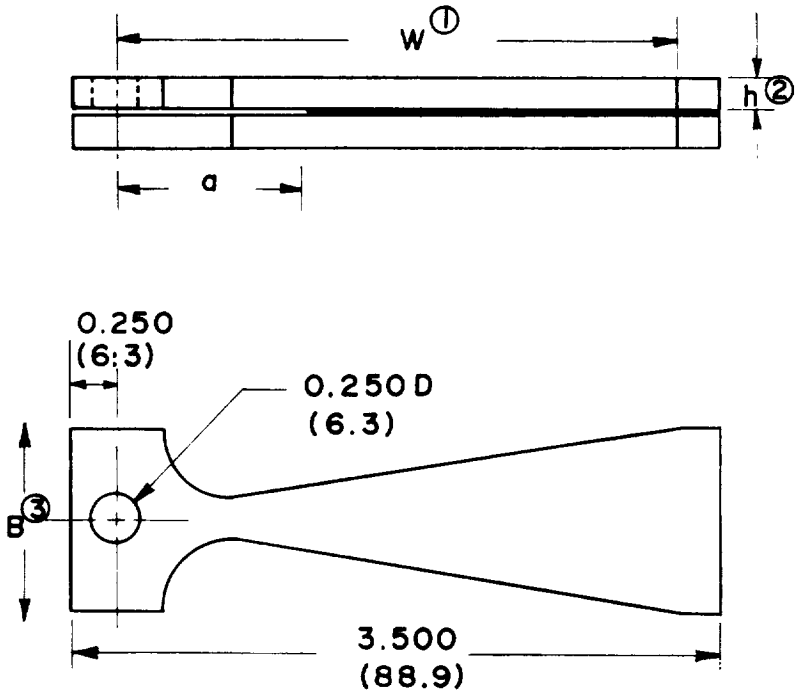

NOTES: ① W = 3.000 (76.2)
② h = 0.125 (3.2)
③ B = 1.000 (25.4)

Fig. 7 WTB specimen geometry. All dimensions are inches (mm).

way no special effort is required to be certain that the displacements being measured are those from the load line. The details of this loading arrangement are shown in Appendix C.

To prevent the load rod from coming into contact with the access hole in the top adherend as the specimen is opened, its nose was tapered. A simple calculation (see Fig. 8) of geometrically wedging the loading rod in the top adherend for the worst case specimen (WTB specimen with an adherend modulus of 5.2×10^6 psi, i.e., 35.8 GPa) showed that the projected diameter, d_p, decreases by 95 percent, while the rotation of the adherends causes an offset, e, of approximately 0.17 inches (4.4 mm) at a displacement of 1.0 inch (25 mm). The loading rod geometry shown in Fig. C-2 would physically wedge at this displacement. Wedging effects were not noticed during this program for displacements less than about 0.5 inches (13 mm). Since the WTB specimen equilibrium load is well established well before this displacement, the wedging problem was of little practical importance in the current study. However, this potential problem can be completely eliminated by replacing the hole in the top adherend with a slot. The slot geometry would also allow easier loading of the specimen into the test fixture.

3.3.2 Compliance Measurement of WTB Specimens

Aluminum alloy 2024-T73 was used as the adherend for the compliance measurement. Six specimens were prepared with initial crack lengths ranging from 3/8 inch to 2¼ inch (9.5 mm to 57 mm) following the procedure outlines in Appendix D. Each specimen was loaded, removed from the test fixture and re-loaded six times. The reported compliance is the average of these trials. A standard deviation of five percent was observed at each crack length tested. As the WTB specimen compliance is proportional to the crack length squared [see eq. (2-8)], the results were plotted on this scale, in Fig. 9. A linear least squares regression was used to determine the coefficients in an equation of the from:

$$C = \beta + \alpha a^2 \qquad (2\text{-}9)$$

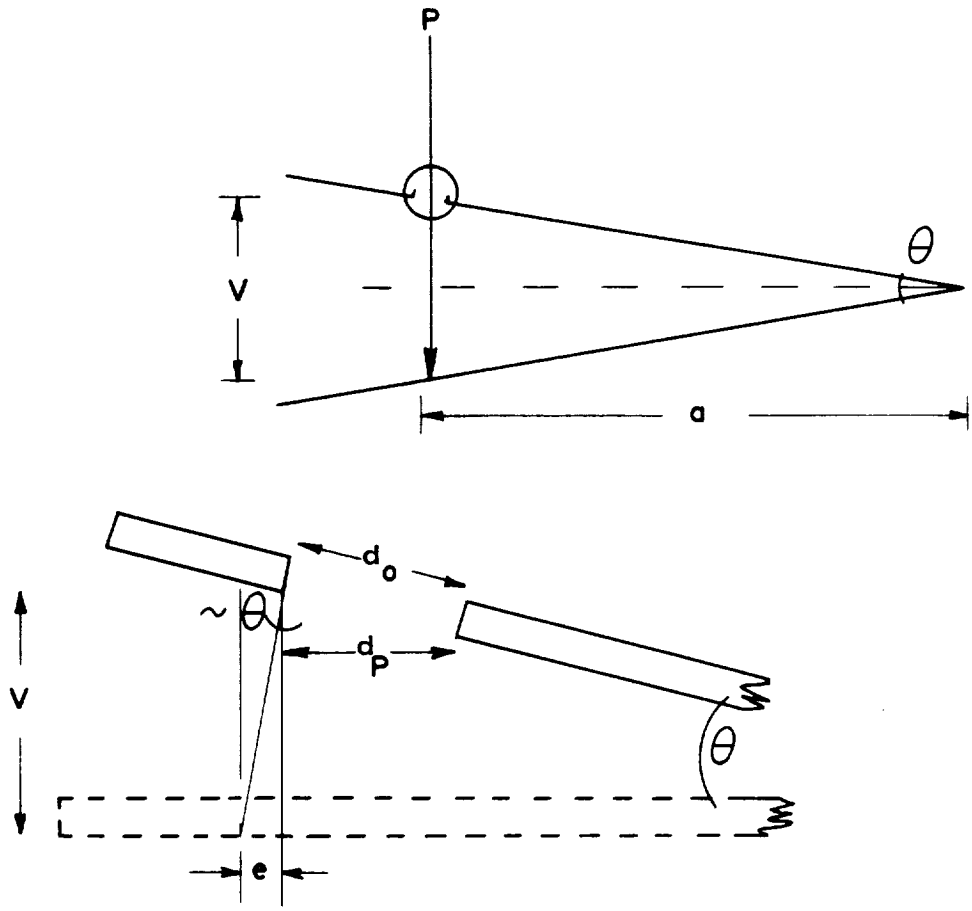

$$\text{WEDGING} = \text{PROJECTION} + \text{OFFSET}$$

$$= (d_o - d_p) + e/2$$

$$= d_o(1 - \cos\theta) + 1/2\, V \tan\theta, \quad \theta = \tan^{-1}\left(\frac{V}{2a}\right)$$

Fig. 8 Geometrical wedging of the loading rod during the opening of a cantilever beam specimen.

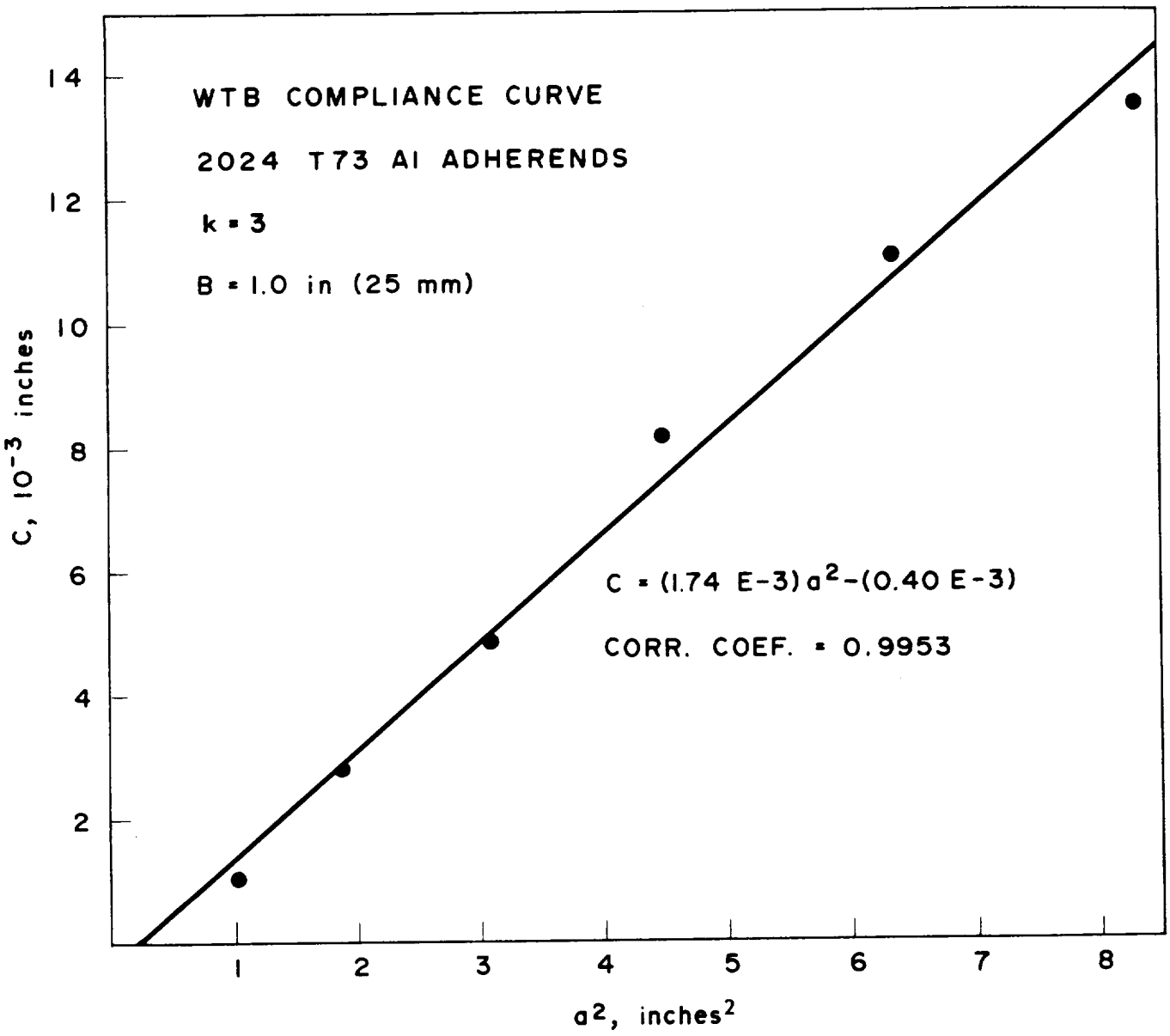

Fig. 9 WTB specimen [k = 3, B = 1.0 inch (25 mm)] compliance.

A correlation coefficient of greater than 0.99 statistically confirms what is obvious from the plot. It is noteworthy that the intercept, β, is nearly zero, and that the fitted slope $\alpha = 1.74 \times 10^{-3}$ $(in\text{-}lb)^{-1}$ is identical to the theoretical value, $\alpha = 12k/Eh^3$.

3.3.3 WTB Test Results and Fractography

Test results for the WTB specimen composite adherends are summarized in Table III. Fractographs of the first four specimens are shown in Fig. 10. These four specimens were made with adherends that were cleaned, but not roughened. As was the case for the UDCB specimens, specimens made from composite A showed a greater tendency to separate at the adhesive-composite interface than the B composite.

Subsequently, the composite specimen surfaces were roughened with 400 grit SiC paper to help prevent adhesive failure. Figure 11, which contains the fractographs for this series of tests, shows that the failure mode changed from adhesive failure to wholly interply separation. The fracture in all of these specimens initiated between plies even though an initial unbonded area in the adhesive layer was made with "Teflon" tape. It must be noted that all these bonds were thinner than recommended, however. Interestingly, the load-deflection curves remained remarkably flat, even when the fracture plane changed through the adherend thickness from one interply layer to another, as illustrated in Fig. 12 for specimen A-4. Clearly, in this example, the plies in question are not oriented to bear a significant portion of the load in the beam. However, this same phenomenon persists for composite B, where the interply separation removes the 0° fiber from one adherend and effectively adds them to the other (see Fig. 13).

It might also be noted that the $\mathcal{G}$ values fit within the same scatter band when a/h was more than or less than 15. Obviously, the scatter in toughness overshadowed the variation in modulus.

Separation between the plies near the adhesive was also the fracturing behavior found by Han and Koutsky[8] for adhesives using a glass fiber reinforced polyester composite. Bascom, et al.[11] have pointed

Table III

COMPOSITE-ADHESIVE-COMPOSITE TEST RESULTS
FOR WTB SPECIMENS

Outer Ply Orientation	Spec. No.	E 10^6 psi (GPa)	P lbs, (N)	$\mathcal{G}$ lb/in. (N/m)	Primary Failure Mode
45°	A1	5.3 (36.6)	11 (5.0)	0.5 (88)	Adhesive
45°	A2	5.3 (36.6)	10 (4.5)	0.4 (70)	Adhesive
0°	B1	12.3 (84.7)	31 (14.1)	1.6 (280)	Mixed*
0°	B2	12.3 (84.7)	*	--	Mixed*
45°	A3	5.3 (36.6)	20 (9.1)	1.6 (280)	Interply
45°	A4	5.3 (36.6)	20 (9.1)	1.6 (280)	Interply
0°	B3	12.3 (84.7)	23 (10.5)	0.9 (158)	Interply
0°	B4	12.3 (84.7)	29 (13.2)	1.4 (245)	Interply

* Initially adhesive failure transforms into interlaminar ply failure. Specimen No. B1 is primarily adhesive failure, while specimen No. B2 has a larger fraction of its surface with interlaminar separation. There was no region on the load displacement curve where the load remained constant.

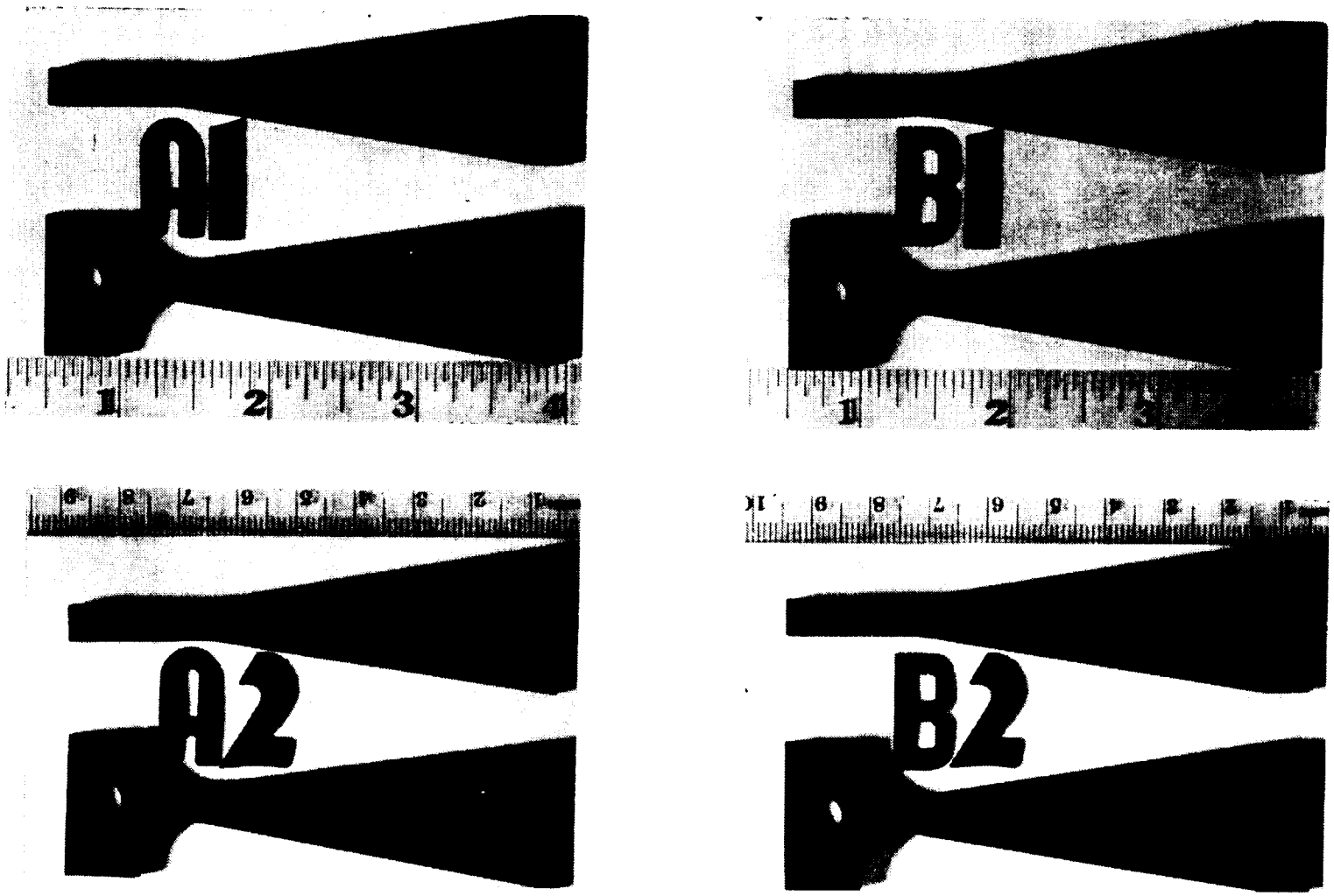

Fig. 10 Fractographs of WTB specimens with similar composite adherends prepared without surface roughening prior to bonding. Prefix of specimen number is composite type.

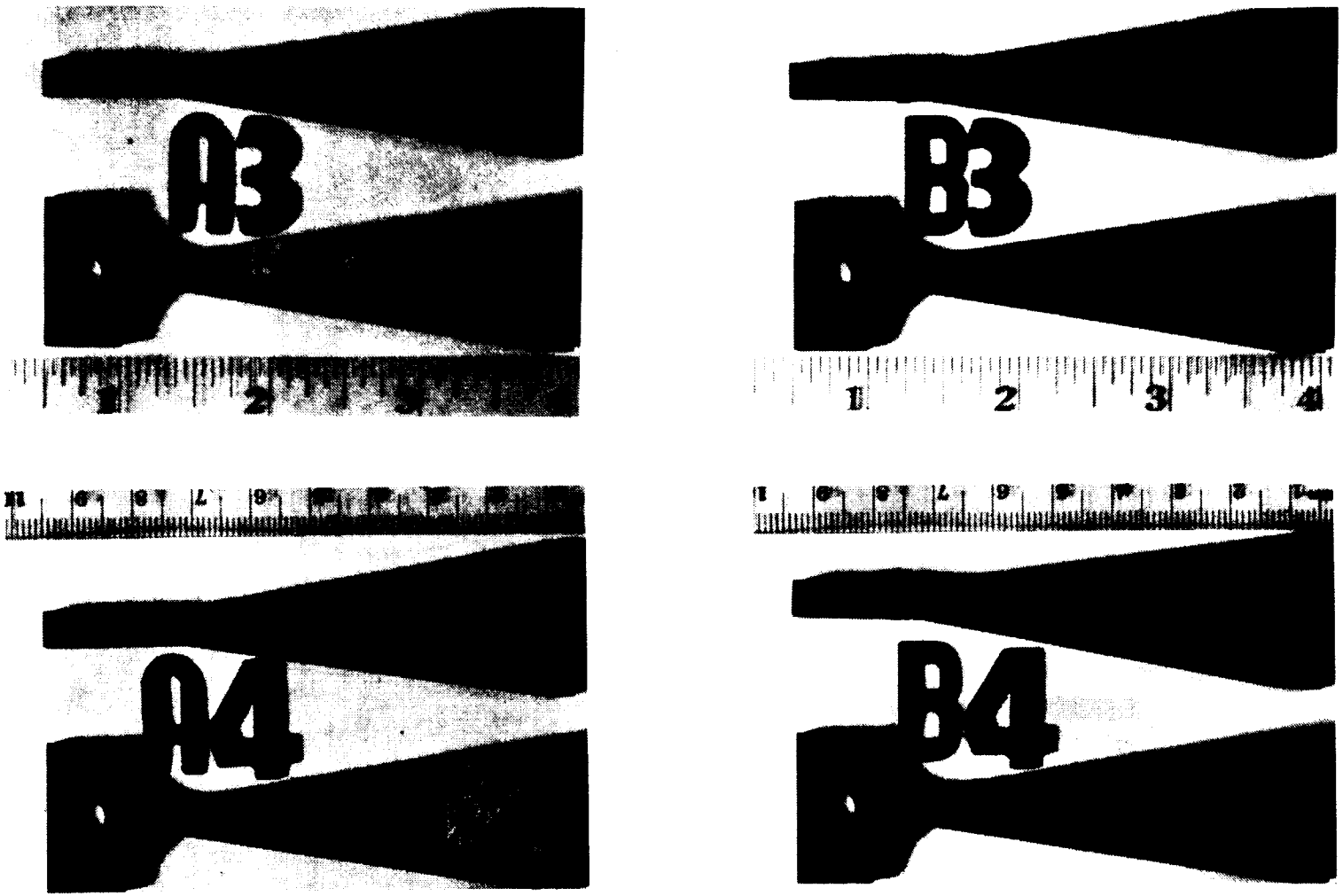

Fig. 11 Fractographs of WTB specimens with similar composite adherends prepared with surface roughening prior to bonding. Prefix of specimen number is composite type.

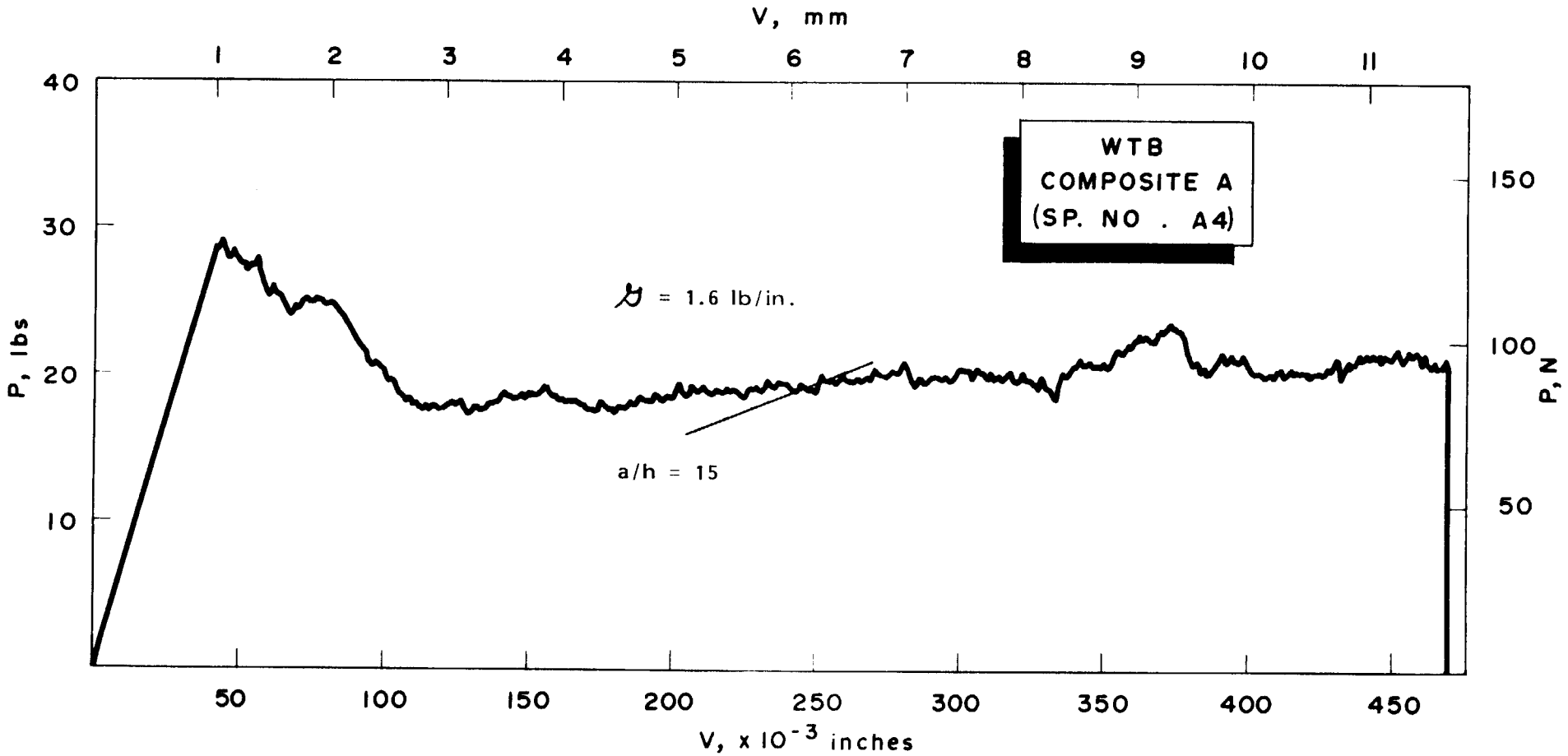

Fig. 12 Typical experimental load-deflection curve for similar composite adherends whose failure mode is 100 percent inter-ply beam failure

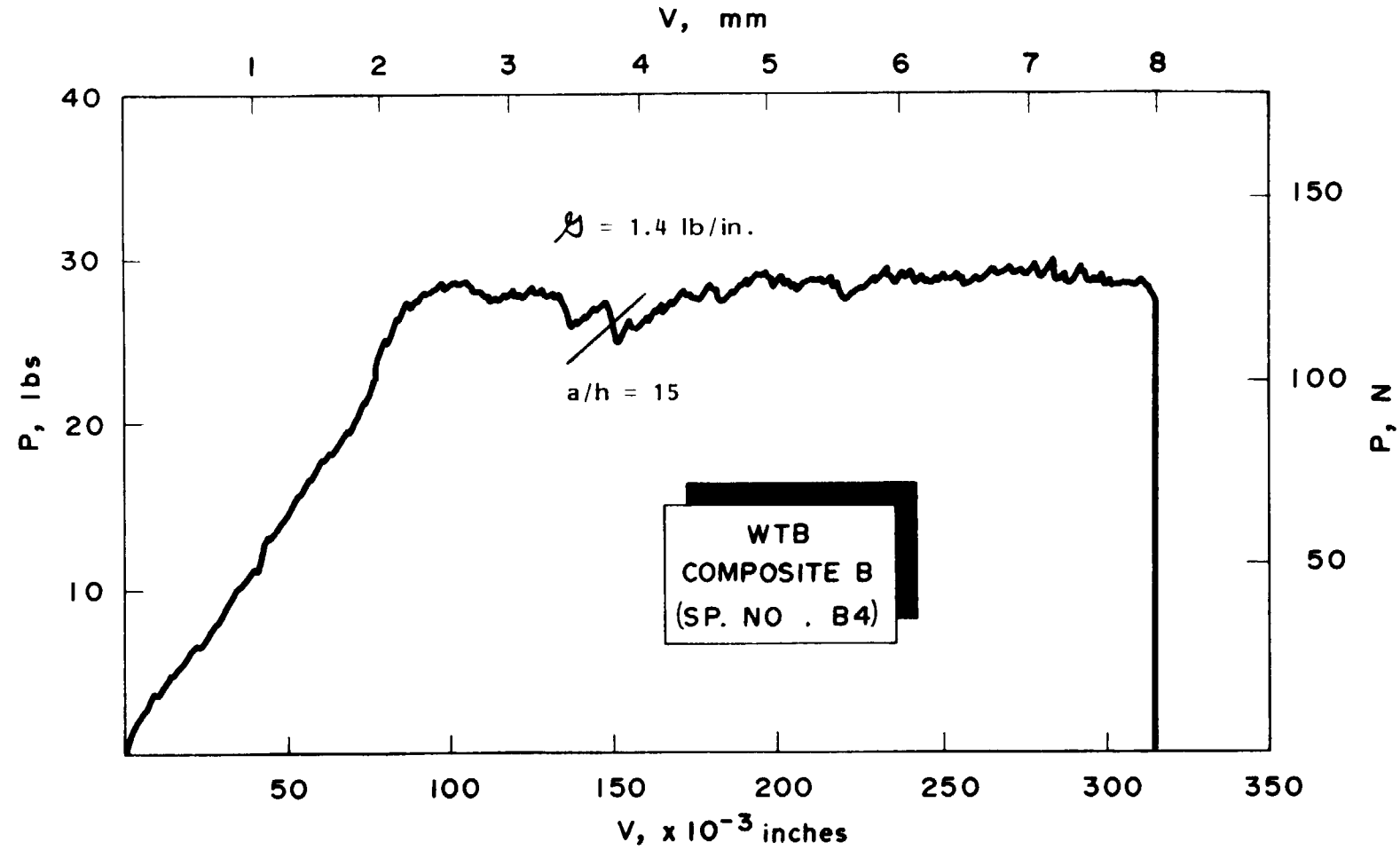

Fig. 13 Typical experimental load-deflection curve for similar composite adherends whose failure mode is 100 percent inter-ply beam failure.

out that the interply toughness of composites is always far lower than the bulk toughness of the matrix resin. They suggest that this behavior occurs because the interply layer is a very thin joint which does not allow the formation of a full deformation zone at the crack tip. If this is the case, the fact that these joints were thinner than recommended did not contribute to the fracture morphology.

4. Conclusions and Recommendations

Uniform and width tapered double cantilever beam specimens were used to measure the fracture toughness of adhesive joints made with composite adherends. Both types of test specimen were designed to take into account the fact that the bending elastic modulus of composites is a function of span-to-depth ratio. A novel method for loading thin-adherend DCB specimens was introduced in which the load-point displacement measuring device was also the loading member.

For well made joints, the crack appeared to initiate and propagate between the plies near the adhesive joint for monotonically increasing loads even though a starter flaw was placed in the adhesive. This behavior was also reported for adherends made of a glass fiber reinforced polyester composite[8]. It has been suggested that a resin matrix in a composite will always have a lower value of toughness than its bulk value because the interply layer is a thin joint that does not allow for the development of a full deformation zone at the crack tip[11].

Additional Mode I opening load tests will be conducted with other than monotonically increasing loads to determine whether or not the interplies always have lower crack propagation resistance than the adhesive layer under opening mode conditions. Furthermore, joint configurations that do not allow interply separation will also be examined.

REFERENCES

1.a. E. J. Ripling, H. T. Corten and S. Mostovoy, "Fracture Mechanics: A Tool for Evaluating Structural Adhesives," J. Adhesion, Vol. 3, pp 107-123 (1971). (Also published in SAMPE Journal, 1970.)

1.b. S. Mostovoy, C. R. Bersch and E. J. Ripling, "Fracture Toughness of Adhesive Joints," J. Adhesion, Vol. 3, pp 125-144 (1971).

1.c. E. J. Ripling, S. Mostovoy and C. Bersch, "Stress Corrosion Cracking of Adhesive Joints," J. Adhesion, Vol. 3, pp 145-163 (1971). (Also published in SAMPE Journal, 1970.)

2. S. Mostovoy and E. J. Ripling, "Flaw Tolerance of a Number of Commercial and Experimental Adhesives," Adhesion Science and Technology, Vol. 9B, pp 513-562.

3. T. R. Brussat and S. Mostovoy, Fracture Mechanics for Structural Adhesive Bonds,, Final Report for Contract No. F33615-75-C-5224 (15 June 1975 - 15 July 1977), Technical Report No. AFML-TR-77-163, Air Force Materials Laboratory, Wright-Patterson AFB, OH 45433.

4. "Standard Recommended Practice for Fracture Strength in Cleavage of Adhesives in Bonded Joint," ASTM Standard D3433-75, 1979 Annual Book of ASTM Standards, Part 22: Wood; Adhesives, American Society for Testing and Materials.

5. S. Mostovoy, P. B. Crosley and E. J. Ripling, "Use of Crack-Line-Loaded Specimens for Measuring Plane Strain Fracture Toughness," J. of Materials, Vol. 2, (1967), pp 661-681.

6. T. R. Brussat, S. T. Chiu and S. Mostovoy, Fracture Mechanics for Structural Adhesive Bonds, Tenth Interim Report, Contract No. F33615-75-C-5224, Air Force Materials Laboratory, Wright-Patterson AFB, OH 45433.

7. D. F. Devitt, R. A. Schapery and W. L. Bradley, A Method for Determining the Mode I Delamination Fracture Toughness of Elastic and Viscoelastic Composite Materials, J. Composite Materials, Vol. 14, (1980), pp 270-285.

8. K. S. Han and J. Koutsky, "The Interlaminar Fracture Energy of Glass Fiber Reinforced Polyester Composites, submitted to J. Composite Materials.

9. C. Zweben, W. S. Smith and M. W. Wardle, "Test Methods for Fiber Tensile Strength, Composite Flexural Modulus, and Properties of Fabric-Reinforced Laminates," Composite Materials: Testing and Design (Fifth Conference) ASTM STP 674, S. W. Tsai, Ed. American Society for Testing and Materials, (1979), 228-262.

10. "Standard Test Method for Flexural Properties of Plastics and Electrical Insulating Material," ASTM Standard D790-71 (Reapproved 1978), 1979 Annual Book of ASTM Standards, Part 35: Plastics - General Test Methods, Nomenclature, American Society for Testing and Materials.

11. W. D. Bascom, J. L. Bitner, R. J. Moulton and A. R. Siebert, "The Interlaminar Fracture of Organic-Matrix Woven Reinforced Composites," Composites (1980), pp 9-18.

Appendix A

DEMONSTRATION THAT $\mathcal{G}$ DEPENDS ON BEAM CROSS SECTION AT THE CRACK TIP

Double cantilever beam (DCB) specimens can be analyzed as a pair of opposed built in beams. Consider the bending of the beam shown in Fig. A-1. The curvature is given by

$$y'' = \frac{M}{EI} = \frac{Px}{EI} \qquad (A-1)$$

the slope by,

$$y' = \int_x^a \frac{Px}{EI}\, dx \qquad (A-2)$$

and the deflection by,

$$y = \int_x^a \int_x^a \frac{Px}{EI}\, dx\, dx \qquad (A-3)$$

where,

M = moment (= Px)

E = Young's modulus

I = moment of inertia

A condition of zero slope at x = a has been incorporated in the limits of integration. In general, EI may be considered to be a function of x.

The compliance of a DCB specimen composed of two such beams is taken as

$$C = \frac{2y_o}{P} = \int_o^a \int_x^a \frac{2x}{EI}\, dx\, dx \qquad (A-4)$$

where

y_o = y evaluated at x = 0

Let F be a function such that

$$F(a) - F(x) = \int_x^a \frac{2x}{EI}\, dx \qquad (A-5)$$

or,

$$\frac{dF}{dx} = \frac{2x}{EI} \qquad (A-6)$$

The compliance can then be written

$$C = aF(a) - \int_o^a F(x)\, dx \qquad (A-7)$$

and, upon differentiation,

$$\frac{dC}{da} = aF'(a) \qquad (A-8)$$

or

$$\frac{dC}{da} = \frac{2a^2}{EI}_{x\,=\,a} \qquad (A-9)$$

The noteworthy feature of this result is that, within the limits of beam theory, dC/da, which is the crucial factor in determining $\mathcal{G}$, depends only on the beam dimensions (specifically, on EI) evaluated at the crack front.

A more complete description takes into account shear deformation of the beam. In this case

$$\frac{dC}{da} = \frac{2a^2}{EI} + \frac{6\,(1+\nu)}{EA} \qquad (A-10)$$

where the second term represents the shear contribution to dC/da, and where

ν = Poisson's ratio

A = beam cross-section area

Again, all the quantities are evaluated at the crack front position. For a rectangular beam of height h, $A = 12\, I/h^2$ and

$$\frac{dC}{da} = \frac{2a^2}{EI}\left[1 + \frac{(1+\nu)}{4}\left(\frac{h}{a}\right)^2\right] \qquad \text{(A-11)}$$

Thus, so long as $h/a < 1/8$ and $\nu = 1/3$, the contribution of a shear is less than 1/2 percent.

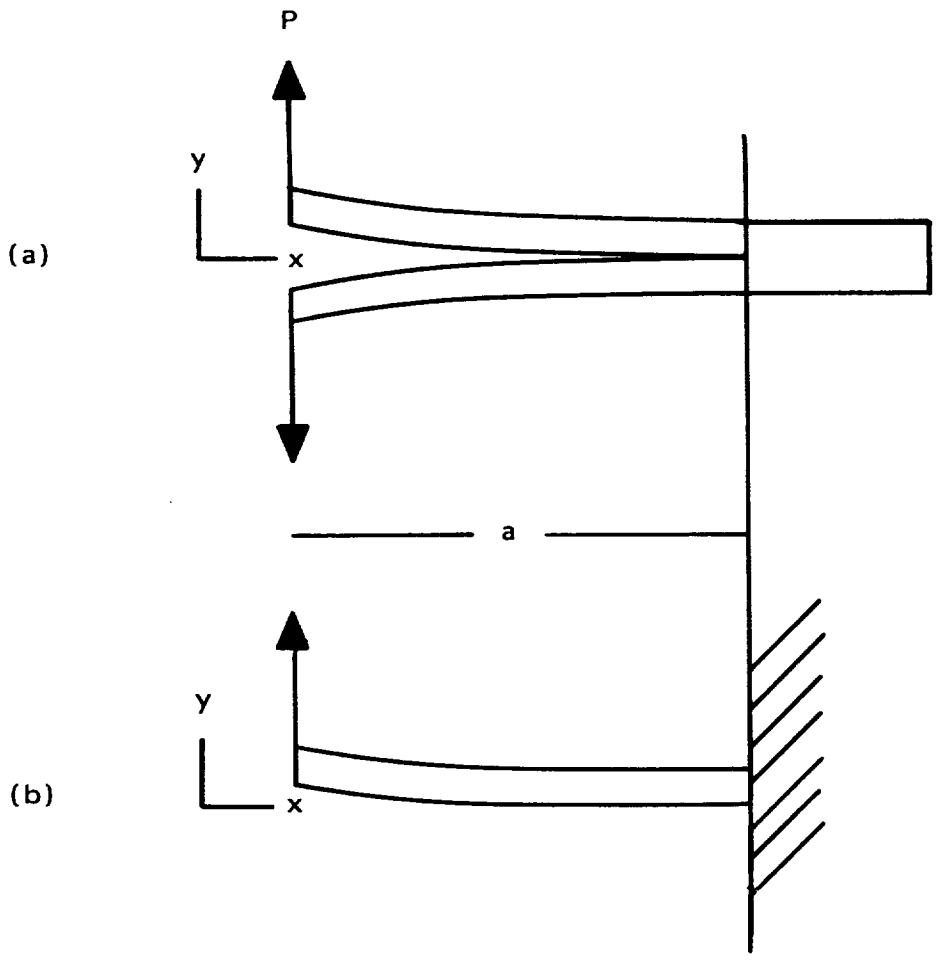

Fig. A1 Nomenclature used to describe the DCB specimen, (a), as a pair of opposed built-in beams, (b).

Appendix B

EFFECT OF CRACK LENGTH DEPENDENT ELASTIC MODULUS ON DCB SPECIMEN BEHAVIOR

For a DCB specimen, the load-displacement relation for a crack propagating at constant $\mathcal{L}$ is given by eq. (2-2) as

$$PV = (2b\mathcal{L}) \cdot (C/C') \tag{B-1}$$

For a specimen in which the apparent tensile modulus, E, depends on crack length, the expression for C is unchanged as long as E is interpreted as the apparent modulus. Because the apparent modulus depends on a, the expression for C' (derivative of C with respect to a) is different.

UDCB Specimen

For the UDCB specimen

$$C = \frac{8a^3}{Ebh^3} \tag{B-2}$$

as given by eq. (2-6), but evaluation of C' gives

$$C' = \frac{dC}{da} = \frac{24\,a^2}{EBh^3}\left[1 - \frac{aE'}{3E}\right] \tag{B-3}$$

where E is the apparent modulus, and $E' = dE/da$. Substituting for C and C' in eq. (B-1) gives

$$PV = (2b\mathcal{L}) \cdot (a/3) \cdot \phi \tag{B-4}$$

where

$$\phi = [1 - aE'/(3E)]^{-1} \tag{B-5}$$

The factor ϕ can be recognized as a correction to the expression, eq. (2-7) obtained for constant E. Substituting the experimentally fitted modulus expression, eq. (3-1) into eq. (B-5) gives

$$\phi = \frac{3\,(a - a_o)}{3a - 4a_o} \tag{B-6}$$

WTB Specimen

For the WTB specimen the experimental compliance was adequately represented by

$$C = \frac{12\,ka^2}{Eh^3} \qquad (B-7)$$

Differentiation with respect to a gives

$$C' = \frac{24ka}{Eh^3}\left(1 - \frac{aE'}{2E}\right) \qquad (B-8)$$

The relationship between P and $\mathscr{G}$ as given in eq. (2-1) is

$$P^2 = (2b\mathscr{G}) \cdot (1/C') \qquad (B-9)$$

Substituting eq. (B-8) for C' gives

$$P^2 = (2b\mathscr{G}) \cdot \frac{Eh^3}{24ka} \cdot \left(1 - \frac{aE'}{2E}\right)^{-1} \qquad (B-10)$$

Noting that k = a/b gives

$$P^2 = \frac{\mathscr{G}Eh^3}{12k^2}\left(1 - \frac{aE'}{2E}\right)^{-1} \qquad (B-11)$$

The dependence of P on a arises, of course, from the dependence of E on a. Using the E-a relationship given in the test, eq. (3-1) gives

$$P^2 = \frac{\mathscr{G}E_o h^3}{12k^2}\left\{\frac{2\,(a - a_o)^2}{a\,(2a - 3a_o)}\right\} \qquad (B-12)$$

The term in curly brackets represents the correction due to the variable Young's modulus.

Appendix C

PRESS DESIGN FOR LOADING DOUBLE CANTILEVER BEAM SPECIMENS

Figure A-1 illustrates the press designed for use in a conventional mechanical test machine. The purpose of the fixture is to provide a reliable means of applying a load to the bottom adherend of a double cantilever beam concentric with the dowel on which the top adherend rests. The loading rod is machined to a hemisphere of the same diameter of the dowel pins in the fixture. The rod is also tapered from the hemisphere, as shown in Fig. C-2, to prevent it from rubbing the circular opening in the top adherend, which rotates as the specimen is opened. Thus, both halves of the double cantilever beam specimen are free to rotate with this design. Figure C-3 shows the fixture with an LVDT coil attached to the top. The magnetic core is an integral part of the load rod (Fig. C-2) and provides a direct measure of the load line displacement. Figure C-3(b) illustrates that the loading rod shoulder drops to the top adherend after the specimen fractures. The LVDT was chosen to have a one inch (25 mm) range based on the calculated WTB deflections for aluminum adherends (10.5×10^6 psi, i.e., 72 GPa modulus).

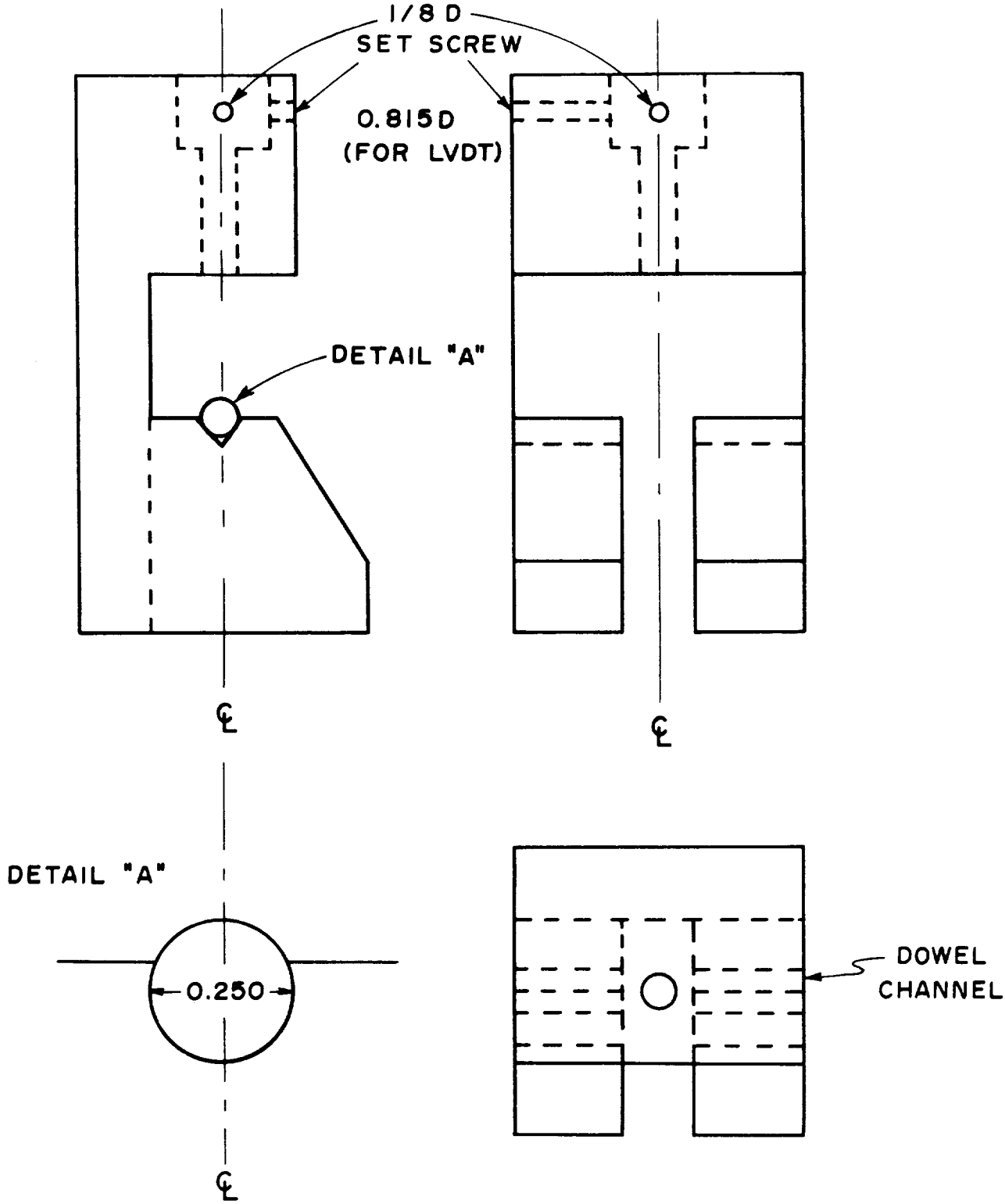

Fig. C1 Point loading adhesive testing fixture (1/1 scale).

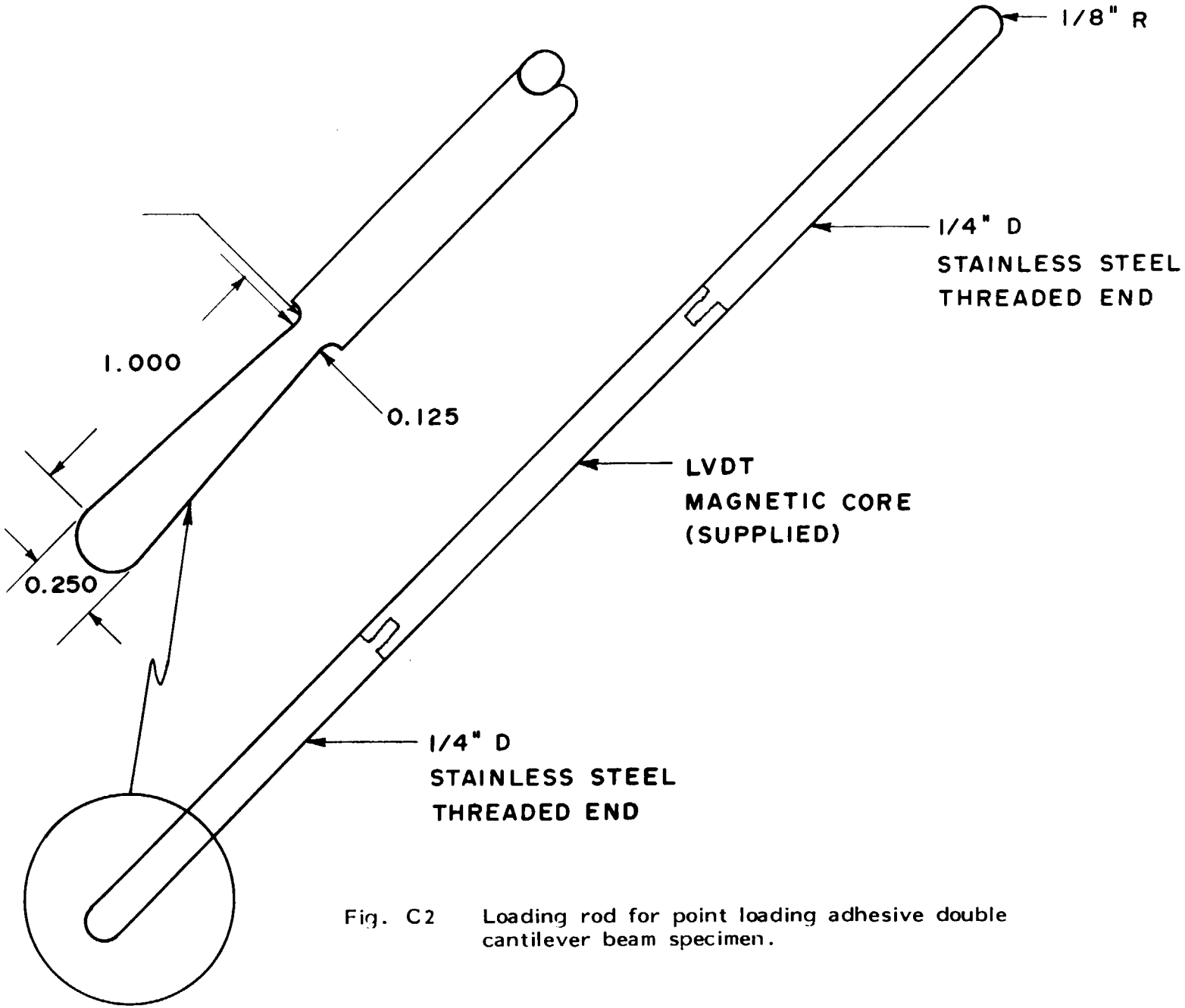

Fig. C2 Loading rod for point loading adhesive double cantilever beam specimen.

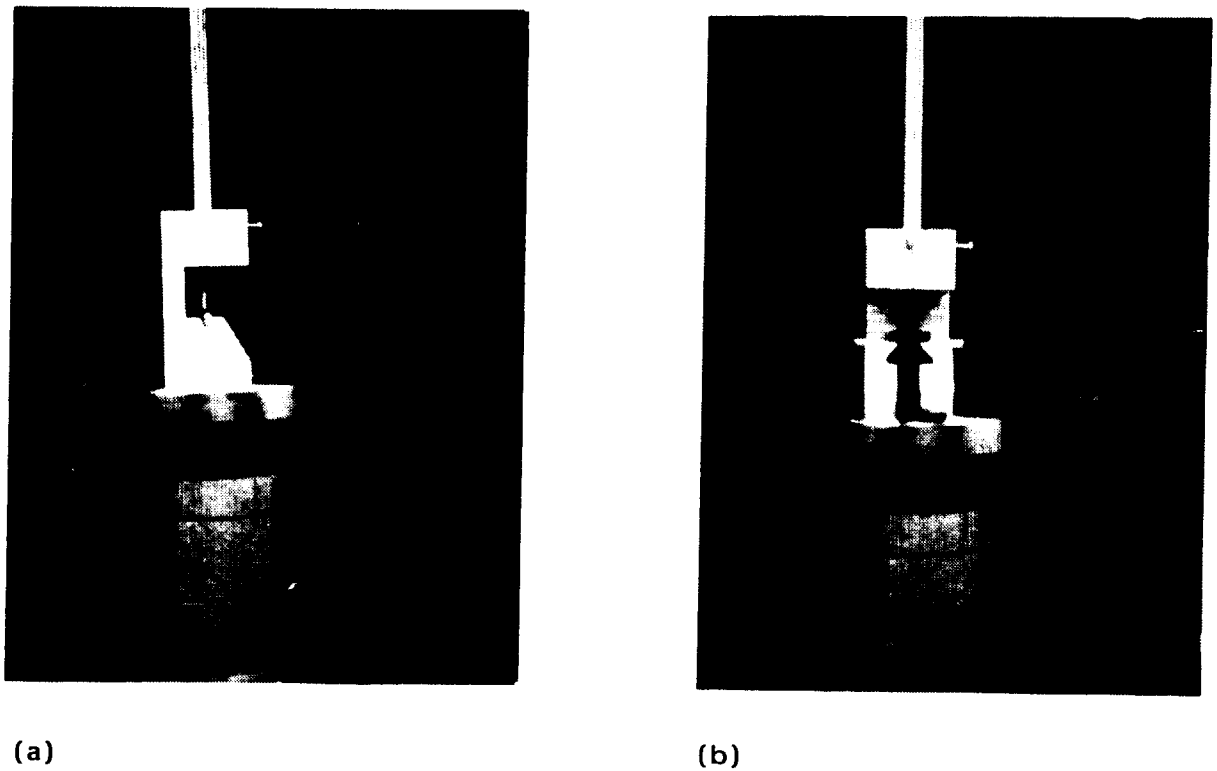

(a) (b)

Fig. C-3 Point Loading Adhesive Testing Fixture with LVDT attached to top (a) side view (b) front view.

Appendix D

PROCEDURE FOR PREPARING WIDTH TAPERED BEAM (WTB) ADHESIVELY BONDED SPECIMENS

1. Prepare pre-adhesive blanks with the geometry shown in drawing D-1.

2. Ultrasonically clean the pre-adhesive blanks by immersion in a non-aqueous solvent bath. For non-metallic adherends, follow the standard recommended practice for preparing surfaces of plastics prior to adhesive bonding: ANSI/ASTM D2093-69 (Reapproved 1976). For titanium adherends, the stabilized phosphate-fluoride treatment (method I-S) is used. For aluminum adherends, the phosphoric acid anodizing treatment is used.

3. The bonding conditions prescribed by the adhesive manufacturer are followed on the WTB pre-adhesive blanks with the exception of pressure which is reduced by half to minimize run out. Two alignment holes are provided at the end of the specimen to prevent the bottom adherend from slipping relative to the top during the cure cycle. It is not necessary to use this precaution when a press is used.

4. The specimen is machined to the final configuration shown in drawing D-2. Sawing the taper angle into the previously bonded top and bottom pre-adhesive blanks provides a uniform, smooth surface between the adherends and the adhesive. The machining conditions can be adjusted to accommodate the adherend material; plastic, non-metallic composite, metallic composite, or metal.

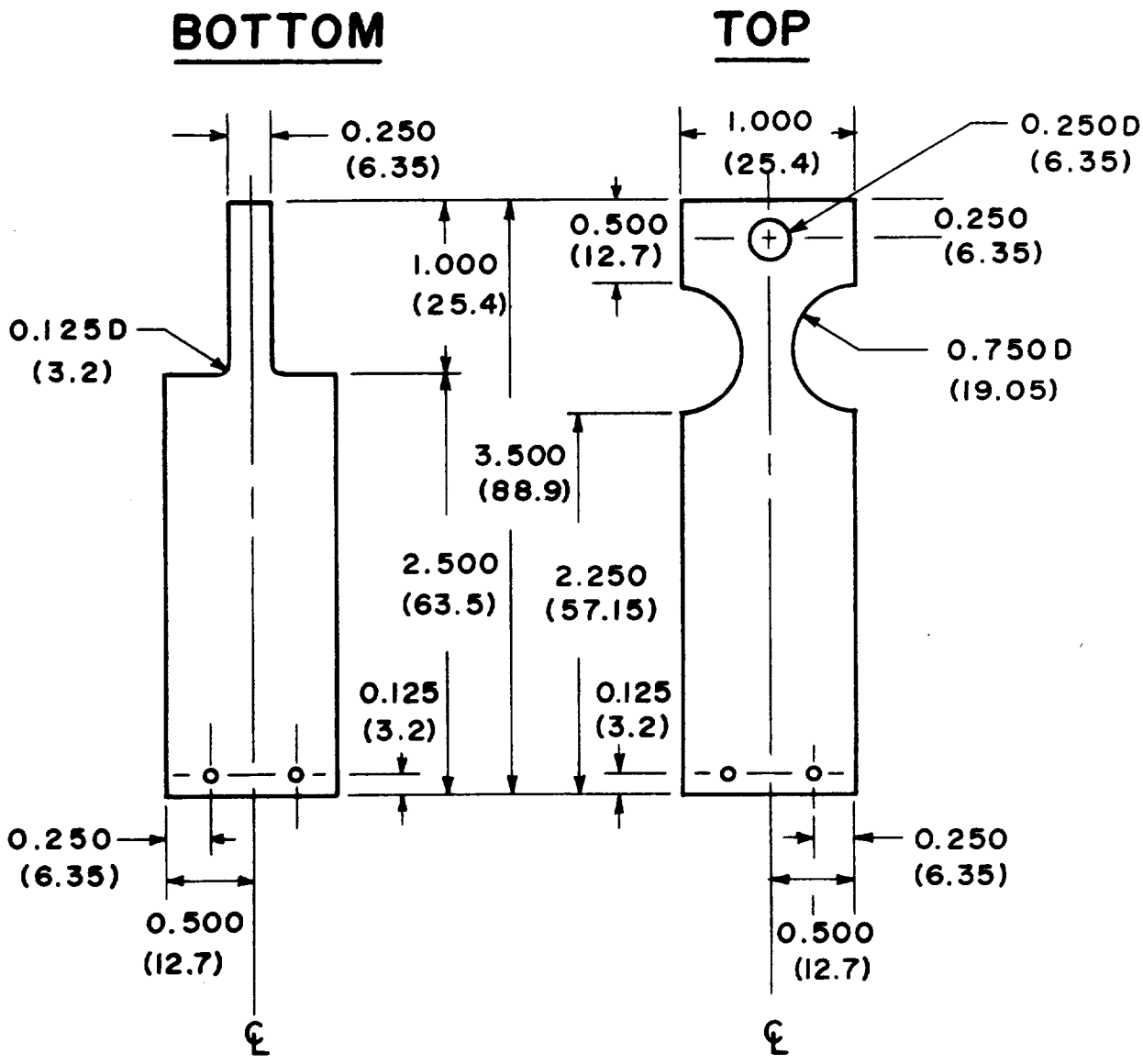

Fig. D1 WTB specimen pre-adhesive blanks. Dimensions are inches (mm).

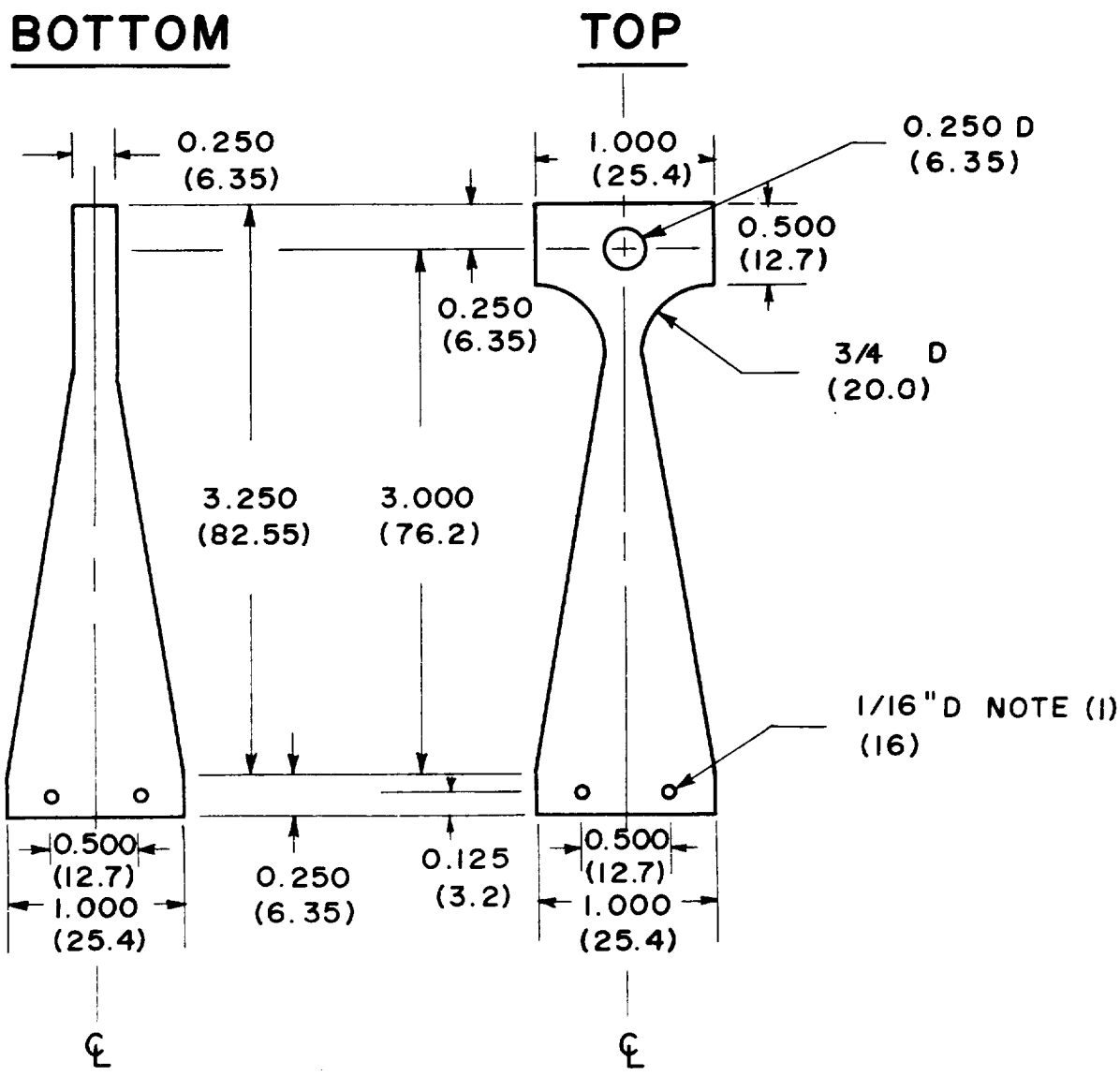

NOTES:

① 1/16" D ALIGNMENT

② DIMENSIONS ARE INCHES (mm)

Fig. D2 WTB specimen design.

Distribution List

W. F. Brown, Jr.
NASA Lewis Research Center
Mail Stop 49-6
21000 Brookpark Road
Cleveland, OH 44135

Tito Serafini
NASA Lewis Research Center
Mail Stop 49-1
21000 Brookpark Road
Cleveland, OH 44135

Structural Mechanics & Polymers Branch
NASA Lewis Research Center
21000 Brookpark Road
Cleveland, OH 44135

John H. Crews, Jr.
NASA Langley Research Center
Mail Stop 188-E
Hampton, VA 23665

Larry Roderick
NASA Langley Research Center
Hampton, VA 23665

Norman Johnston
NASA Langley Research Center
Hampton, VA 23665

Dr. Herb Leybold
Head of Composites
Primary Structures Project Office
NASA Langley Research Center
Hampton, VA 23665

Charles F. Bersch
NASA
Attn: Mail Code RTM-6
Washington, DC 20546

Lt. Col. Joe Morgan
Director of Aerospace Sciences
AFOSR
Building 410
Bolling AFB, DC 20332

Dr. W. B. Jones
AFWAL/MLBC
Wright-Patterson AFB, OH 45433

Weldon Scardino
AFWAL/MLT
Wright-Patterson AFB, OH 45433

Dr. G. Sendeckyj
AFFDL/FBEC
Wright-Patterson AFB, OH 45433

Plastics Technical Evaluation Center
ARRADCOM
Dover, NJ 07801

Ray Wegman
ARRADCOM
Dover, NJ 07801

J. M. Bodnar
ARRADCOM
Samuel Feltman Ammunition Lab.
Dover, NJ 07801

Solomon Goldfein
USAMERDC AMXFB RML
Material Research Division
Bldg. 363
Fort Belvoir, VA 22060

John C. Hurt, Assoc. Dir.
Metallurgy & Materials Science Div.
U. S. Army Research Office
P. O. Box 12211
Research Triangle Park, NC 27709

Aero Vehicle Department
Naval Air Development Center
Attn: Materials Lab & Structures Lab
Warminster, PA 18974

John Gurtowsky
NAVAIR
AIR-52032A
Washington, DC 20360

Naval Surface Weapons Center
Attn: Code WO-31
White Oak, MD 20910

Naval Ship Engineering Center
Attn: Code 6101E
Washington, DC 20360

Naval Ship R&D Center
Attn: Code 725
Washington, DC 20007

Dr. Willard D. Bascom
Aerospace Div.
Hercules, Inc.
8132 TR
Bacchus Works
Magna, UT 84044

Dr. T. R. Brussat
7452/63G/A1
Lockheed California Co.
Burbank, CA 91520

A. S. Burhans
Union Carbide Plastics Co.
P. O. Box 670
River Road
Bound Brook, NJ 08805

Robert W. Bushroe
Hughes Aircraft Co.
Mail Station J-3
Bldg. 801, Box 11337
Tucson, AZ 85734

Prof. H. T. Corten
Dept. of Theoretical &
Applied Mechanics
Talbot Laboratory 321C
Urbana, IL 61801

Dr. Nicholas J. DeLollis
Polymer Research & Development
Div. 5813
Sandia Laboratories
Albuquerque, NM 87115

Dennis Donnelly
Materials Engineer
The Boeing Company
Renton, WA 98055

J. G. Fasold
D/71, Gp. 522, Bldg. 7
Columbus Aircraft Div.
Rockwell International
4300 E. Fifth Avenue
Columbus, OH 43216

Donald Flaggs
Lockheed Palo Alto Research Labs.
Dept. 5233, Bldg. 205
3251 Hanover Street
Palo Alto, CA 94304

Prof. M. Fourney
School of Engineering
UCLA
Los Angeles, CA 90024

R. Freyer
Grumman Aerospace Corp.
Bethpage, NY 11714

Dr. John Gardon
M & T Chemicals, Inc.
26701 Telegraph Road
Southfield, MI 48076

Prof. A. N. Gent
Institute of Polymer Science
University of Akron
Akron, OH 44325

Dr. F. P. Gerstle
Sandia Laboratories
Div. 5844
Albuquerque, NM 87115

Dr. Robert H. Gillespie
U. S. Dept. of Agriculture
Forest Service
Forest Products Laboratory
P. O. Box 5130
Madison, WI 53705

John Hart-Smith
McDonnell Douglas Corp.
Douglas Aircraft Company
Long Beach, CA 90801

G. Havilland/D/115
Rockwell International
Los Angeles Int'l. Airport
Los Angeles, CA 90009

Dr. Richard Hertzberg
Lehigh University
Materials Research Center
Coxe Lab, #32
Bethlehem, PA 18015

Dr. James R. Huntsberger
E. I. du Pont de Nemours & Co.
Experimental Station 323/108
Wilmington, DE 19898

Dr. M. I. Jacobson
Manager, Manufacturing Research
Orgn. 47-01, Bldg. 150
Lockheed Missiles and Space Co.
Sunnyvale, CA 94086

Dr. O. K. Johannson
Research Department
Dow Corning Corp.
Midland, MI 48640

E. A. Jolley
Bell Helicopter
P. O. Box 11000
Amarillo, TX 79105

D. H. Kaelble
Rockwell Science Center
1049 Camino Dos Rios
Thousand Oaks, CA 91360

Stephen L. Kaplan
Arthur D. Little, Inc.
Acorn Park
Cambridge, MA 02140

Dr. Keith T. Kedward
Chief, R&D Structures Analysis
M.Z. 42-6810
General Dynamics
Convair Division
San Diego, CA 92138

Dr. Frank Kelley
Institute of Polymer Science
University of Akron
Akron, OH 44325

Max Klotzsche
Douglass Aircraft Co.
3855 Lakewood Blvd.
Long Beach, CA 90801

Prof. W. G. Knauss
Mail Code 205-50
California Institute of Technology
Pasadena, CA 91125

Prof. James Koutsky
Dept. of Chemical Engineering
University of Wisconsin
Madison, WI 53706

Robert L. Kosarek
Alcoa Technical Center
Alcoa Center, PA 15069

Dr. Ray B. Kreiger, Jr.
American Cyanamid Company
Bloomingdale Dept.
Havre de Grace, MD 21078

Dr. A. Kremheller
Dept. 72-14
Zone 402
Lockheed-Georgia Company
Marietta, GA 30060

Dr. R. Levy
McDonnell Douglas Res. Lab.
Dept. 221-22
St. Louis, MO 63166

Materials
Research
Laboratory,
Inc.

Dr. Armand Lewis
Hughson Chemical
Lord Corporation
2000 West Grandview Blvd.
Erie, PA 16512

Prof. James L. Lubkin
Dept. of Civil Engineering
Michigan State University
East Lansing, MI 48823

John Lucas, Chief
Structures & Materials
Sikorsky Aircraft
Stratford, CT 06602

Dr. John A. Manson
Lehigh University
Materials Research Center
Coxe Lab. #32
Bethlehem, PA 18015

Prof. James W. Mar
Aeronautics & Astronautics Dept.
MIT
Cambridge, MA 02139

Prof. Jovan Mijovic
Dept. of Chemical Engineering
Polytechnic Institute of New York
333 Jay Street
Brooklyn, NY 11201

A. K. Miller
supervisor Analytical Group
Boeing Commercial Airplane Co.
Boeing Materials Technology
Seattle, WA 98100

L. E. Meade
Lockheed-Georgia Company
Marietta, GA 30063

Dr. A. G. Metcalfe
Solar Aircraft Co.
2200 Pacific Highway
San Diego, CA 92112

Prof. S. Mostovoy
Dept. of Materials and Metallurgy
IIT
Chicago, IL 60616

Prof. F. McGarry
Massachusetts Institute of Technology
Cambridge, MA 02139

Bob Nagle
B. F. Goodrich Company
500 S. Main Street
Akron, OH 44318

Dr. J. S. Noel
Texas A&M University
Civil Engineering Dept.
College Station, TX 77844

Dr. James Noland
American Cyanamid Co.
1937 W. Main Street
Stamford, CT 06904

Dominick C. Novelli
LMSC
Dept. 71-31, Bldg. 103
P. O. Box 504
Sunnyvale, CA 94086

Prof. John Outwater
University of Vermont
Burlington, VT 05401

R. J. Palmer
Douglas Aircraft Company
Mail Code 1-18
3855 Lakewood Blvd.
Long Beach, CA 90801

Prof. T. Byron Pipes
University of Delaware
Newark, DE 19711

Dr. John T. Quinlivan
Boeing Materials Technology
Commercial Airplane Group
Mail Stop 73-43
P. O. Box 3707
Seattle, WA 98124

Reinforced Plastics Division
Minnesota Mining & Mfg. Co.
2501 Hudson Road
St. Paul, MN 55119

Dr. James Renton
Vought Corporation
Advanced Technology Center
P. O. Box 6144
Dallas, TX 75222

Dr. J. L. Rutherford
Research Center
General Precision, Inc.
1150 McBride Avenue
Little Falls, NJ 07424

Dr. Richard E. Robertson
Ford Motor Company
Scientific Research Staff
P. O. Box 2053
Dearborn, MI 48121

Ms. Elisa Rogers
LSMC
Dept. 74-83, Bldg. 360
P. O. Box 551
Burbank, CA 91520

Dr. John Romanko
General Dynamics
Structures and Materials Technology
MZ 5984
Fort Worth, TX 76101

R. Sabia
Bell Telephone Laboratories, Inc.
Murray Hill, NJ 07971

Dr. Richard A. Schapery
Civil Engineering Dept.
Texas A & M University
College Station, TX 77843

Dr. H. C. Schjelderup
Douglas Aircraft Co.
3855 Lakewood Blvd.
Long Beach, CA 98046

H. Siegel
McDonnell Aircraft Co.
P. O. Box 516
St. Louis, MO 63166

Dave Sims
Bell Helicopter Co.
Dept. 80
P. O. Box 482
Fort Worth, TX 76101

Ms. Vivan Yang Steger
Senior Research Engineer
General Dynamics Corp.
P. O. Box 80847
San Diego, CA 92138

Sam Sterman
Union Carbide Corporation
Silicones Division
P. O. Box 44
Tonawanda, NY 14152

Paul Stifel
McDonald Aircraft Co.
Dept. 247, Bldg. 33
P. O. Box 516
St. Louis, MO 63166

Dr. Norman Sunshine
Whittaker Corp.
600 Victoria Street
Costa Mesa, CA 92627

Dave Wangsness
3M Center
Bldg. 209-1CW
St. Paul, MN 55144

Carl Weber
B. F. Goodrich Co.
Research Center
Brecksville, OH 44141

Dave Wilhem/3853 Zone 82
Northrop Corp./Aircraft Div.
3901 West Broadway
Hawthorne, CA 90250

Materials
Research
Laboratory,
Inc.

Dr. M. L. Williams
Dean of Engineering
University of Pittsburgh
Pittsburgh, PA 15261

Dr. Ed M. Wu
University of California
Lawrence Livermore Laboratory
P. O. Box 808 (L-342)
Livermore, CA 94550

Dr. D. A. Yurek
3M Center
Bldg. 209-1 CW
St. Paul, MN 55101